

Q1 A mud-dominated coastal plain to lagoon with emerged carbonate mudbanks: †The imprint of low-amplitude sea level cycles (mid-Upper Cretaceous, South Iberian Ramp)

Q3/Q2

 The corrections made in this section will be reviewed and approved by a journal production editor.

Diego Torromé*, dtorrome@unizar.es, Marcos Aurell, Beatriz Bádenas

Departamento de Ciencias de la Tierra-IUCA, Universidad de Zaragoza, 50009 Zaragoza, Spain

*Corresponding author.

Editor: Dr. Moretti Massimo

Abstract

The middle Santonian-lower Campanian carbonate-mud dominated succession deposited in the northeastern margin of the South Iberian Ramp (La Cañadilla Fm, NE Spain) shows a complex set of interfingering facies developed in a low-energy and low-gradient shallow-marine to coastal environment. Three facies belts characterize the environment reconstructed in this work: (1) a low-energy shallow marine lagoon dominated by radiolitic rudist limestones and miliolid-rich facies with variable carbonate-mud content; (2) a transitional belt with a patchy distribution of ponds and mudbanks. This belt mostly consists of miliolid-rich limestones with variable amount of fenestral porosity, which are interfingering with charophytes and gastropod marls and limestones usually mixed with miliolids; (3) a coastal plain with strong freshwater influence characterized by the sedimentation of marls and limestones with charophytes, gastropods and root traces and intraclastic/black pebble limestones. The studied succession is arranged in high-frequency sequences, including meter-scale parasequences bounded by widespread flooding surfaces, which stack in five larger-scale shallowing-upward sequences (6–20 m thick). The time calibration of these sequences obtained from strontium isotopes and biostratigraphic data (benthic foraminifera) suggests a major control in the sedimentation by climate-driven low-amplitude sea level oscillations formed in tune with the long- and short-eccentricity orbital cycles. Cyclic sea level rises controlled the existence of widespread flooding events in the low-gradient carbonate ramp at the onset of parasequences, which in the studied marginal areas of the South Iberian Ramp were mostly sourced from the southern Tethyan realm. Therefore, the La Cañadilla Fm provides an example of a complex shallow marine to coastal system giving rise to a mosaic distribution of carbonate-mud dominated facies, with sedimentation mostly influenced by external factors resulting in a well-defined stratigraphic architecture. The similarities with modern analogous systems such as the Ten Thousand Islands of the Florida Bay are discussed in this paper.

Keywords:

Carbonate facies, Coastal, Orbital cycles, Upper Cretaceous, Iberian Basin

Abbreviations

1.1 Introduction

The Late Cretaceous was a period of active tectonism at a global scale, with enhanced volcanic outgassing and high seafloor spreading rates, which determined global warm climates and high sea levels (e.g. [Hay and Floegel, 2012](#); [Haq, 2014](#)). The gently sloping interior areas of continents were flooded resulting in widespread large epeiric or epicontinental seas ([Pratt et al., 2008](#)). Shallow carbonate environments have been a common topic of discussion for Late Cretaceous rise in sea level helping in the deciphering of the behaviour of these ancient shallow epeiric marine systems (e.g. [Carannante et al., 2000](#); [Simone et al., 2003](#); [Diedrich et al., 2011](#); [Solak et al., 2017](#)). Comparing these shallow marine settings with modern analogues is helpful to understand the controlling factors. However, the present icehouse climate mode and very large (>100 m) Holocene Sea level oscillations (e.g. [Miller et al., 2005](#); [Scotese et al., 2021](#)) contrasting with Cretaceous greenhouse conditions, make difficult to compare with modern analogues to understand how those Cretaceous epicontinental seas behaved.

In this study, the mid-Upper Cretaceous successions of La Cañadilla Fm of the eastern Iberian Basin (South Iberian Ramp, Spain) offers the opportunity to unravel the stratigraphic architecture of a complex mosaic of shallow carbonate facies deposited in a low-energy, gently sloping, coastal plain to shallow marine area. In particular, the paleoenvironment reconstructed for this carbonate-mud dominated formation can be compared with modern analogues such as the carbonate shallow systems of the southern Florida coast ([Lacovara et al., 2003](#)), which has been regarded as a modern analogue of other mud-dominated coastal to shallow carbonates in the stratigraphic record (e.g. [Enos and Samankassou, 2022](#)).


The impact of orbital cyclicity controlling the sedimentary record of high-frequency sequences in Upper Cretaceous marine and continental systems is another point of major interest (e.g. [Liu, 2007](#); [Gil et al., 2009](#); [Segura et al., 2014](#); [Wu et al., 2014](#)). Orbital cyclicity during Late Cretaceous has been important for tracking global anoxic ([Hofmann et al., 2003](#)) and possible glacio-eustasy events ([Al-Husseini, 2018](#)) as proxies for the evolution of carbonate platforms ([Le Goff et al., 2015](#)), and for global correlation of isotopic records ([Thibault et al., 2016](#)).

Previous work on La Cañadilla Fm provided general stratigraphic and sedimentological features ([Canerot et al., 1982](#); [Almunia et al., 1985](#)), but no detailed analysis of facies and high-frequency sequences has been performed so far on this unit. Accordingly, the study of the La Cañadilla Fm in the eastern Iberian Chain presented here has four main purposes: (1) carry out a detailed sedimentological analysis with the reconstruction of a sedimentary model, helping to unravel the lateral and vertical facies distribution after correlation between the different stratigraphic logs; (2) analysis of the observed stratigraphic architecture of La Cañadilla Fm with the identification of parasequences and sequences bounded by flooding surfaces of regional extend; (3) review of the available biostratigraphic information combined with new strontium isotopic data to establish a chronostratigraphic framework of the unit in order to calibrate the duration of the recorded sedimentary cycles and discuss their possible orbital-related origin; (4) compare the obtained data with modern analogues to discuss about processes controlling the sedimentation and response of these shallow marine Iberian epeiric platforms to flooding events.

2.2 Geological Setting

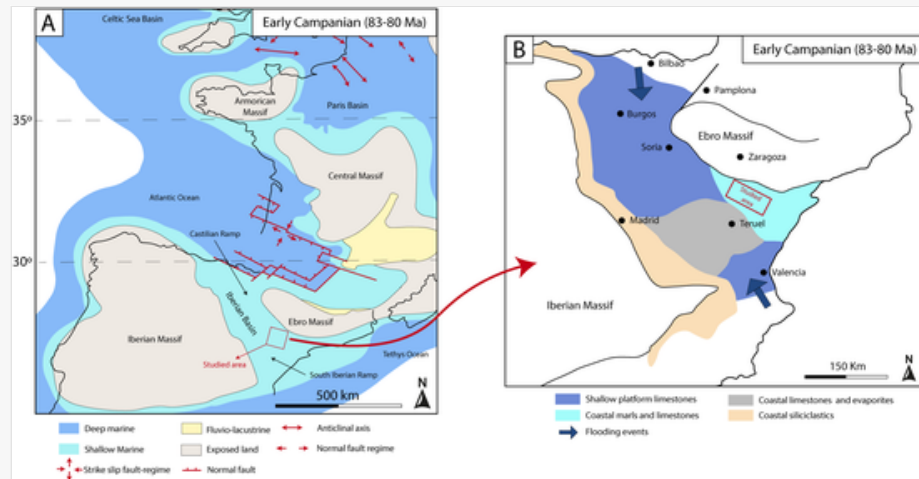
Successive episodes of extensional tectonics related to the western Tethys propagation and Atlantic Ocean opening during the Mesozoic affected the eastern Iberian Plate. As a result, the NW-SE trending intracratonic Iberian Basin Rift System developed. The onset of the formation of this rift system occurred during the Late Permian to Early Triassic rifting phase (e.g. [Arche and López-Gómez, 1996](#); [Sánchez-Moya and Sopeña, 2004](#)). A second latest Jurassic-Early Cretaceous rifting episode involved the formation of several independent sedimentary basins along the Iberian Basin Rift System (e.g. [Salas et al., 2001](#); [Aurell et al., 2019](#); [Aurell et al., 2021](#); [Martín-Chivelet et al., 2019](#)). Afterwards, the Late Cretaceous post-rift stage involved the progressive expansion and homogenization of the depositional areas in

the Iberian Basin (Fig. 1A), with the setting of large carbonate epeiric platforms between the emerged areas of the Iberian and Ebro massifs (Feuillée, 1967; Floquet, 1991).

 Images are optimised for fast web viewing. Click on the image to view the original version.

alt-text: Fig. 1

[Fig. 1](#) [Fig. 1](#)




(A) Paleogeography of western Europe during the early Campanian (modified from Dercourt et al., 2000). (B) Main paleogeographic domains in the Iberian Basin during the early Campanian (compiled from Segura et al., 2004; García et al., 2004 and Martín-Chivelet et al., 2019).

During the Late Cretaceous, the Iberian Basin was located in a paleolatitude of 25°N–30°N (Dercourt et al., 2000). A hot climate fluctuated from arid to sub-humid, depending on the influence of the Subtropical High Belt and the equatorial system of ocean currents which controlled the displacement of warm waters towards higher latitudes through the Tethys Ocean (e.g. Skelton, 2003; Stampfli and Kozur, 2006; Hay and Floegel, 2012; Martín-Chivelet et al., 2019). Sea surface temperature estimates for Iberian seas varies from 24 to 31 °C (Pucéat et al., 2003; Steuber et al., 2005). In the Iberian Basin, two large marine domains opened towards the Bay of Biscay and the Tethys Sea referred as the Castilian Ramp and the South Iberian Ramp respectively (Fig. 1A; Martín-Chivelet et al., 2019).

The coastal to shallow marine carbonate-dominated successions studied here accumulated in an area of the South Iberian Ramp attached to the emerged Ebro Massif (Fig. 1B). Shallow-marine platform carbonates with frequent presence of rudists dominated to the northwest and southeast of the basin, whereas coastal carbonates, marls and evaporites accumulated in the central hinge area between the Castilian and the South Iberian ramps (Segura et al., 2004; Martín-Chivelet et al., 2019). The episodic connections between the Castilian Ramp and the South Iberian Ramp during the early and mid-Late Cretaceous generated a temporary shallow marine seaway through central Iberia (e.g. Floquet, 1991; Alonso et al., 1993; Martín-Chivelet et al., 2002). The relative homogeneous tectonic subsidence in the Iberian Basin during the Late Cretaceous favoured a major role in the sedimentation of the episodic marine transgressions (Alonso et al., 1993; Segura et al., 2001; Gil et al., 2004, 2006). Third-order relative sea level fluctuations and higher-order orbital cycles were recorded as transgressive-regressive cycles and higher-order sequences, both in the shallow platform settings of the Castilian Ramp (e.g. Floquet et al., 1982; Gräfe, 1994, 1999; Floquet, 1991, 1998, 2004; Segura et al., 2001, 2014; Baceta et al., 2004), and in the South Iberian Ramp (Martín-Chivelet and Giménez, 1992; Martín-Chivelet, 1995, 2003).

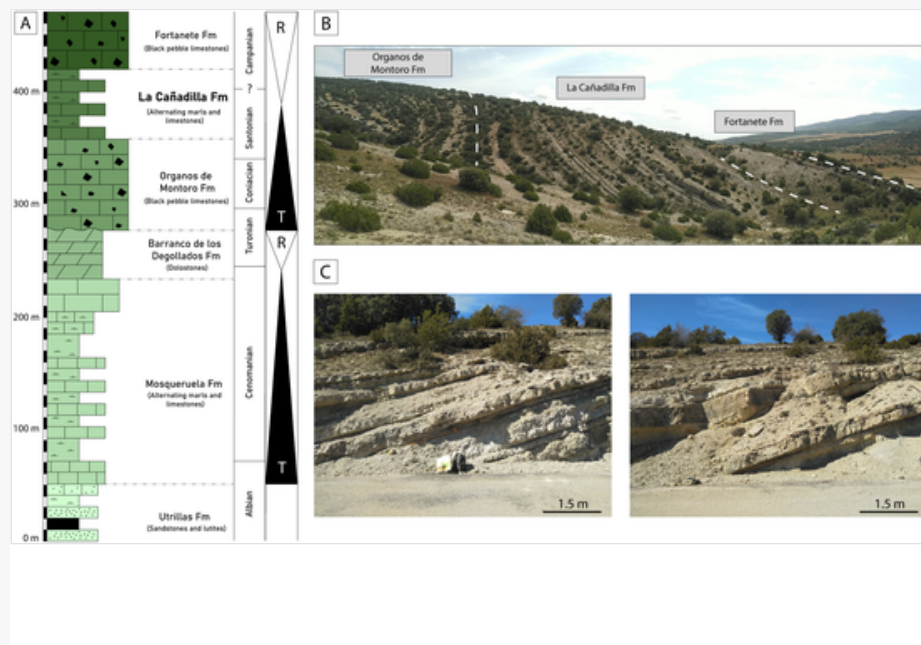
The uppermost Cretaceous coastal carbonate-dominated successions studied here accumulated in the northeastern marginal areas of the South Iberian Ramp, and belong to the so-called La Cañadilla Fm. This unit consist of a 30–60 m-thick, well-bedded succession of marls and micritic to skeletal limestones (Fig. 2). Based on biostratigraphic data (radiolitic rudists and benthic foraminifera) and regional correlation, the La Cañadilla Fm was assigned in previous works to the latest Coniacian-early Maastrichtian (Canerot et al., 1982), or to the Santonian-middle Campanian (Almunia et al., 1985), or to the late Santonian-early Campanian (Gil et al., 2004; García et al., 2004). The unit is

included in the major mid-Turonian to Campanian second-order transgressive-regressive (T-R) cycle (Alonso et al., 1993; Segura et al., 2004). In the studied sector of the South Iberian Ramp, the La Cañadilla Fm embraces the transgressive peak of this major T-R cycle (Fig. 2; Almunia et al., 1985). Moreover, the La Cañadilla Fm represents a third-order sequence bounded by regional unconformities (Segura et al., 2004). The lower boundary with the underlying Organos de Montoro Fm is a regional flooding surface associated with an abrupt facies change from coastal palustrine meter-thick breccias to dm-thick alternations of skeletal limestones and marls. The upper boundary with the Fortanete Fm represents a major regressive event marked by the widespread deposition of coastal palustrine to lacustrine breccias. The Fortanete Fm is bounded on top by a major regional discontinuity involving the initiation of continental terrigenous sedimentation in alluvial fans to fluvial systems in isolated intramountain basins (e.g. Montalbán and Aliaga subbasins: Fig. 3), related to the onset of the Alpine orogeny (e.g. González and Guimerá, 1993; Casas et al., 2000).


 Images are optimised for fast web viewing. Click on the image to view the original version.

alt-text: Fig. 2

[Fig. 2](#)

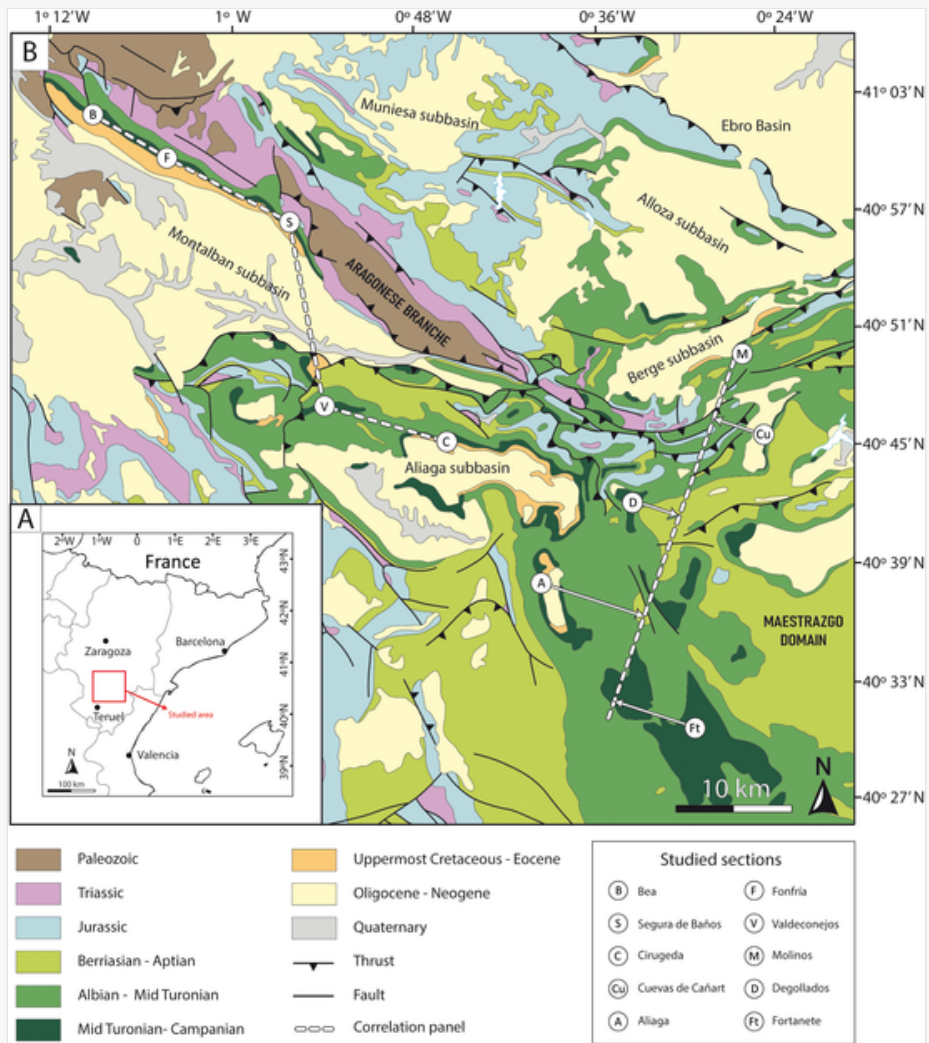


(A) Synthetic stratigraphic log of the Upper Cretaceous in the northeastern part of the South Iberian Ramp, indicating the distribution of the two major T-R cycles defined in Segura et al. (2004). (B) Panoramic view of the Beal log indicating the distribution of the Organos de Montoro, La Cañadilla Fm and Fortanete formations. (C) Outcrop views of the Fonfría log showing the typical alternating marls and limestones that characterize La Cañadilla Fm.

 Images are optimised for fast web viewing. Click on the image to view the original version.

alt-text: Fig. 3

[Fig. 3](#)



Geological map of the study area (modified from Rodríguez et al., 2008) showing the location of the 10 logged sections and the two reconstructed correlation panels.

3.3 Materials and methods

A bed-by-bed analysis of the La Cañadilla Fm has been performed in ten detailed stratigraphic logs, distributed in a 40 × 80 km wide area located within the Aragonese branch and Maestrazgo domains of the Iberian Chain (Fig. 3). The area extends from the locality of Bea (log B, northwest), to Fortanete (log Ft, southeast), with an average distance between logs of about 13 km. The thickness of the unit ranges from 30 m in Molinos (log M), to up to 61 m in Fortanete (log Ft).

Facies description was carried out combining field observations of bedding, lithology, texture, components and sedimentary structures, complemented with the analysis of samples, including the petrographic study of limestones in 185 polished sections and 200 thin sections, and 50 marl samples for description of microfossil content and analysis of the %CaCO₃. Textural classification of limestones follows the [Dunham \(1962\)](#) and [Embry and Klovan \(1971\)](#) schemes. [Flügel and Munnecke \(2010\)](#) and [Pettijohn et al. \(2012\)](#) were used for description and terminology of non-skeletal grains.


The definition of high-frequency sequences of different orders in every stratigraphic log followed two main different criteria: vertical evolution of facies and the presence of sharp (locally erosional) surfaces that reflect sedimentation breaks linked to significant platform flooding events (e.g. [Bosence et al., 2009](#); [Bádenas et al., 2010](#); [Sevillano et al., 2020](#)). Two log correlation panels including a 40 km-long NNE-SSW trending transect and a c.50 km-long NW-SE transect ([Fig. 3](#)) were constructed to decipher the lateral continuity of facies and sequences. The distance between logs and the absence of intermediate continuous outcrops do not allow the physical tracing of the sequences between logs (e.g. [Bádenas et al., 2010](#)), so that correlation of sequences was based on the best fit considering facies trends within sequences (e.g. [Sevillano et al., 2020](#)).

To constrain the age of the studied unit, six well-preserved rudist shells found in two selected localities (Cirugeda and Degollados, [Fig. 3](#)) were sampled for strontium-isotopic analysis. Rudist shells were examined under a binocular microscope before drilling to carry out the geochemical analysis. Those areas of the shells most susceptible to diagenetic alteration or that appeared altered under the binocular microscope (microfractures, chalky-cloudy areas and the exterior parts in contact with sediment) were removed with a dental drill. The ⁸⁷Sr/⁸⁶Sr ratio was determined with a TIMS-Phoenix thermal ionization mass spectrometer at the *CAI Geocronología y Geoquímica Isotópica* of the *Universidad Complutense de Madrid* (Spain). Isotopic data were corrected for possible ⁸⁷Rb interferences and were normalised to a value of 0.1194 for ⁸⁷Sr/⁸⁶Sr in order to correct possible mass-fractionation. During the period of analysis, the NBS-987 standard gave an average ⁸⁷Sr/⁸⁶Sr value of 0.710245 ± 0.000019, which was used to correct the measured values from a possible deviation referred to the standard. The analytical error of the ⁸⁷Sr/⁸⁶Sr ratio referred to 2σ was 0.01%.

4.4 Facies analysis

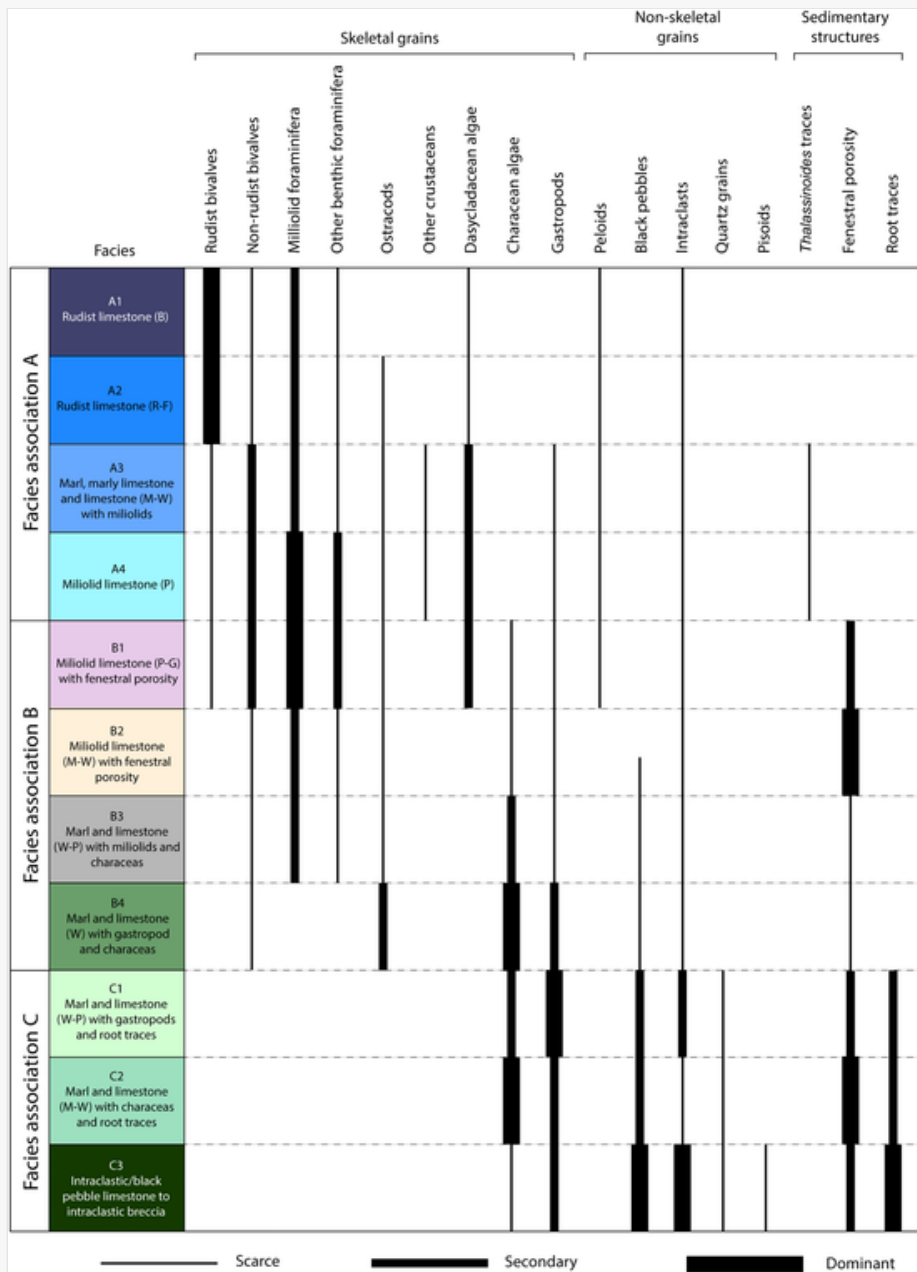
4.1.4.1 Facies description

The coastal to shallow marine carbonate-dominated successions of the La Cañadilla Fm include marls, marly limestones and limestones. Based on texture, components (mainly skeletal grains) and sedimentary structures, eleven facies and three facies associations (A, B, C) have been differentiated ([Fig. 4](#)). Two representative logs, Fonfría and Fortanete, located at the northwest and southeast of the studied area ([Fig. 3](#)), have been selected to illustrate the vertical distribution of facies and facies associations ([Fig. 5](#)). Representative views of thin and polished sections of facies are included in [Figs. 6 to 8](#).


 Images are optimised for fast web viewing. Click on the image to view the original version.

alt-text: Fig. 4

[Fig. 4](#), [Fig. 4](#)

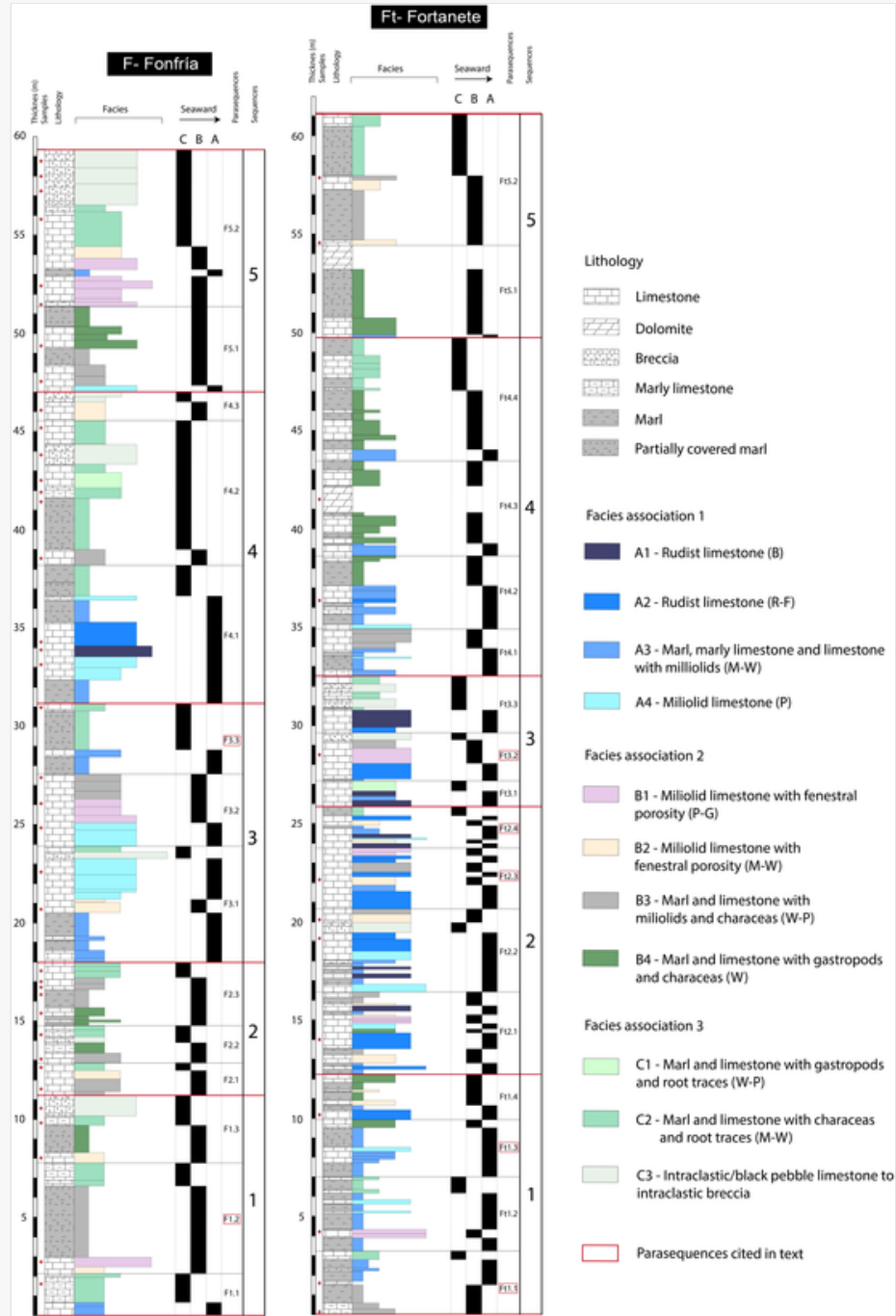


Distribution and relative abundance of skeletal and non-skeletal components, and sedimentary structures in the eleven facies identified in the La Cañadilla Fm.


 Images are optimised for fast web viewing. Click on the image to view the original version.

alt-text: Fig. 5

[Fig. 5, Fig. 5](#)

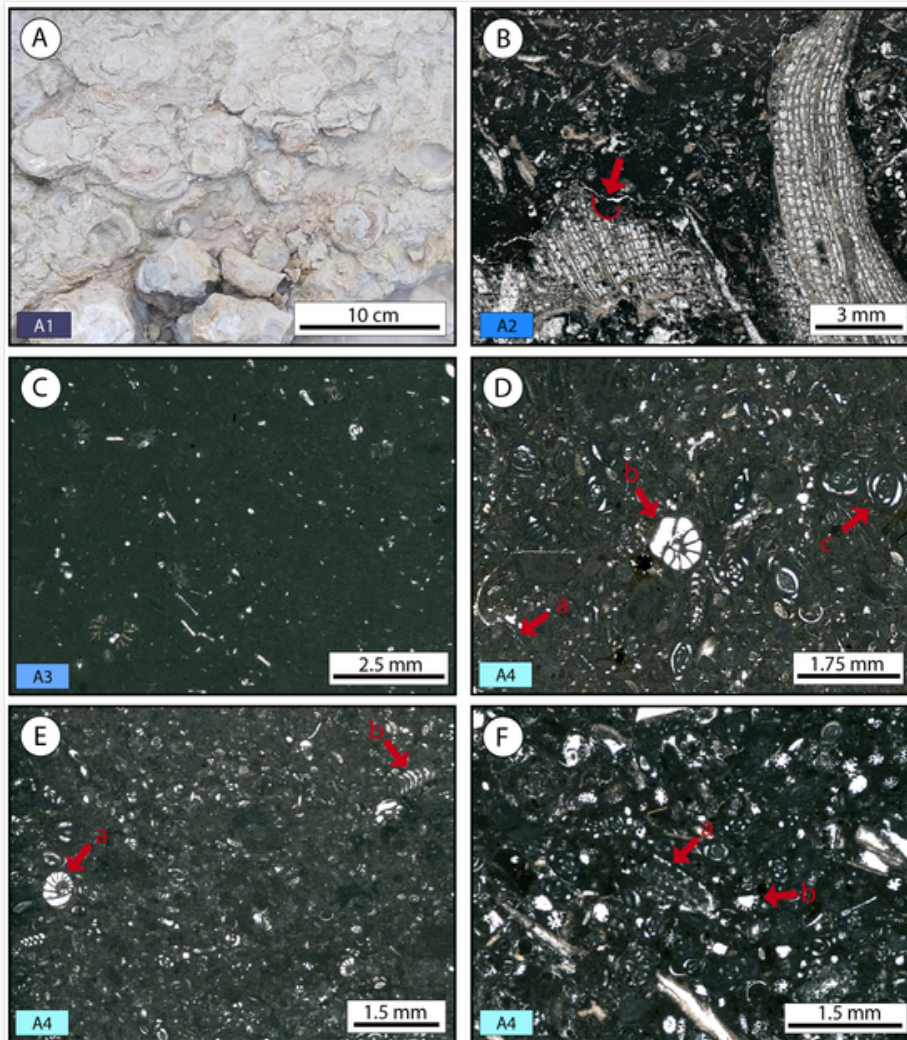


Stratigraphic logs from Fonfría (F) and Fortanete (Ft) displaying the distribution of facies supporting the identification of sequences and parasequences. For description and correlation purposes, parasequences have been named using the log initial followed by the number of sequence, and the number of parasequence (e.g. F1.1, F1.2, F1.3 in sequence 1 in log F-Fonfría).


 Images are optimised for fast web viewing. Click on the image to view the original version.

alt-text: Fig. 6

Fig. 6, Fig. 6

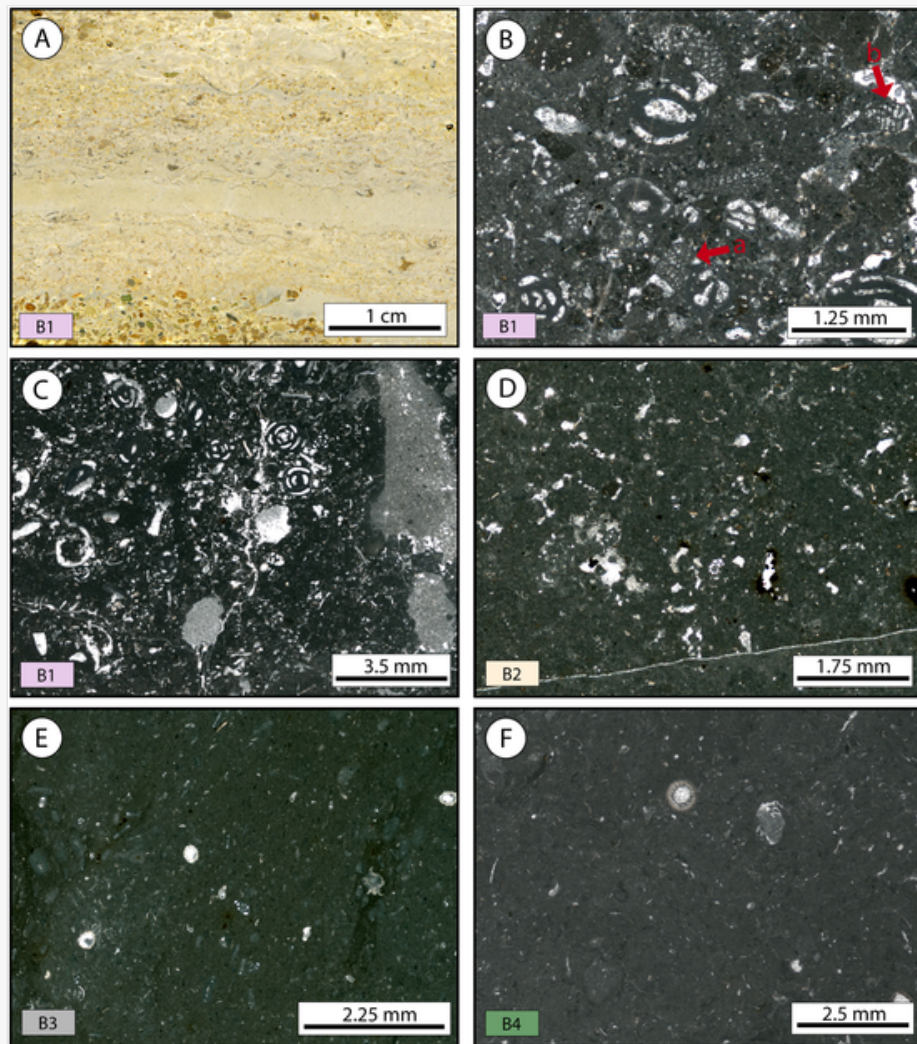


(A) Facies A1 (Valdeconejos log, parasequence C3.3) showing in-situ radiolitid rudist banks. (B) Facies A2 (Degollados log, parasequence D3.3) showing fragmented rudist within skeletal facies with miliolids. Arrow points to bioerosion (C) Facies A3 (Valdeconejos log, parasequence V1.1) showing mud-dominated wackestone with dispersed dasyclacean algae (*Clypeina*) and miliolids. (D) Facies A4 (Valdeconejos log, parasequence V1.3) showing miliolid packstone with *Vidalina Hispanica* Schlumberger (a), *Valculamina picardi* Henson (b) and *Quinqueloculina* sp. (c). (E) Facies A4 (Valdeconejos log, parasequence V2.3) showing miliolid packstone with *Peneroplis Giganteus* Gendrot (a) and *Pseudolituonella Mariae* Gendrot (b). (F) Facies A4 (Valdeconejos log, parasequence V4.3) showing miliolid packstone with fragments of *Acicularia* sp. (a, b).


 Images are optimised for fast web viewing. Click on the image to view the original version.

alt-text: Fig. 7

[Fig. 7](#), [Fig. 7](#)

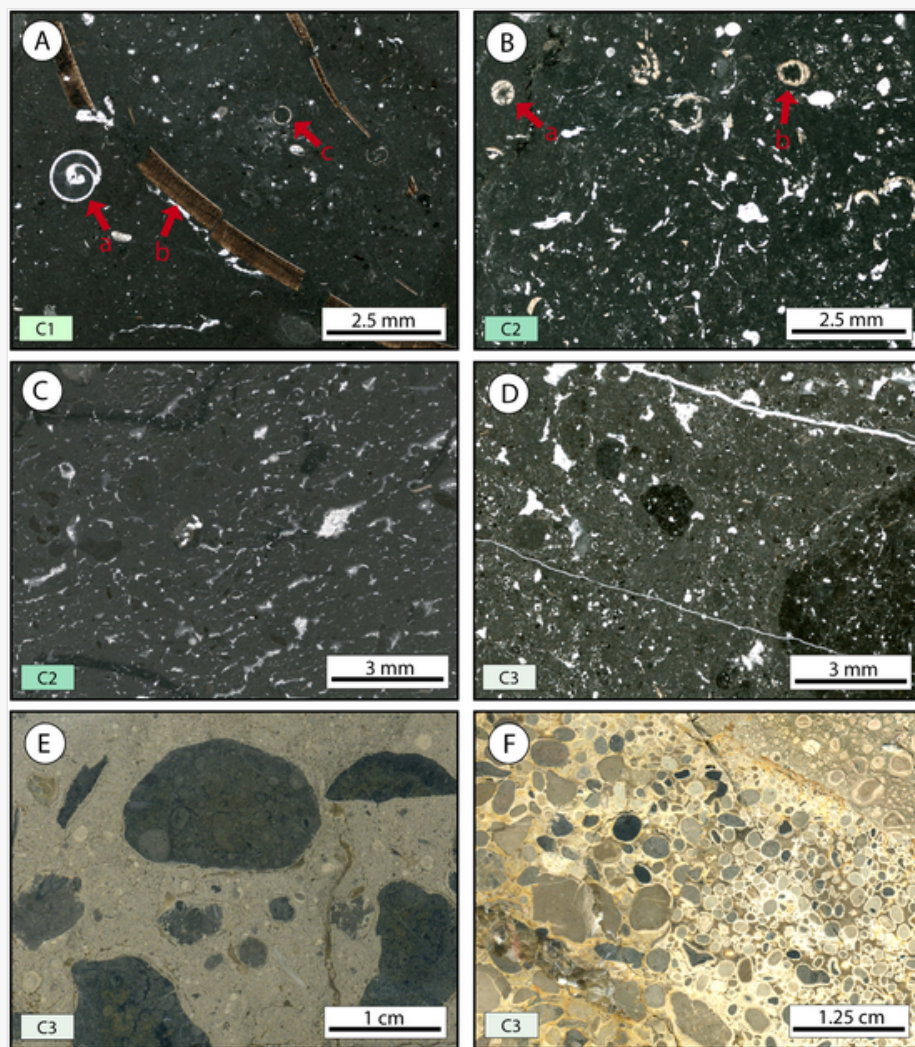


(A) Facies B1 (Molinos log, parasequence M2.2) with graded lamination related to high-energy events. (B) Facies B1 (Fortanete log, parasequence 1.2) showing miliolid packstone with *Cuneolina Conica* D'Orbigny (a) and *Cuneolina Pavonia* Henson (b). (C) Facies B1 (Cirugeda log, parasequence C3.3) showing miliolid packstone with porosity. (D) Facies B2 (Fonfría log, parasequence F3.2) showing miliolid mudstone with porosity. (E) Facies B3 (Valdeconejos log, parasequence 4.1) showing charophytes and miliolid dispersed in a micritic matrix. (F) Facies B4 (Valdeconejos log, parasequence V5.2) with charophytes dispersed in a micritic matrix.

 Images are optimised for fast web viewing. Click on the image to view the original version.

alt-text: Fig. 8

[Fig. 8, Fig. 8](#)



(A) Facies C1 (Bea log, parasequence B4.1) showing a gastropod wackestone with gastropods of variable size (a, b) and charophytes (c). (B) Facies C2 (Aliaga log, parasequence A4.4) showing wackestone with porosity with charophyte gyrogonites (a, b). (C) Facies C2 (Molinos log, parasequence M3.2) showing a mud-dominated textures with well-developed fenestral porosity. (D) Facies C3 (Fonfría log, parasequence 5.2) with black pebbles floating in a micritic matrix with porosity. (E) Facies C3 (Valdeconejos log, parasequence V1.2) showing a grain-supported limestone with big rounded black pebbles. (F) Facies C3 (Aliaga log, parasequence 4.3) showing grain supported textures with coated grains and pisolites.

4.1.1.4.1.1 Facies association A

Facies association A comprises four facies (A1 to A4) characterized by varying abundances of different marine skeletal grains, in particular bivalves (mainly radiolitid rudists), benthic foraminifera (mainly miliolids and in minor proportion lituolids, textularids and rotalids) and dasycladacean algae (*Clypeina* sp., *Acicularia* sp., *Cylindroporella* sp.).

Facies A1 and A2 are rudist-dominated limestones stratified in dm-thick tabular beds. Facies A1 corresponds to rudist boundstones formed by in-situ, entire or partially fragmented, cm-sized rudists (mainly radiolitids) surrounded by a mud-dominated matrix with peloids and scarce micritic mm-sized intraclasts (Fig. 6a). The facies also includes minor proportion of other skeletal grains such as foraminifera, other bivalves and occasionally dasycladacean algae. Facies A2 consists of accumulations of highly fragmented, but poorly rounded rudist shells, either with rudstone or floatstone texture, with a bioclastic wackestone-packstone matrix with foraminifera, and fragmented dasycladacean algae and other bivalves (Fig. 6b). Peloids and micritic mm-sized intraclasts are also locally found.

Facies A3 and A4 are foraminifera-dominated facies, with scarcer rudists and higher proportions of dasycladacean algae compared to rudist facies A1 and A2. Facies A3 is mud-dominated and includes marls, marly limestones and

limestones (wackestones) arranged in tabular (up to 1 m-thick) strata. It is characterized by the relative abundance of miliolids and fragments of non-rudist bivalves and dasycladacean algae (Fig. 6c). Fragmented and entire gastropods, ostracods and disarticulated crabs are also recognized. *Thalassinoides* traces are common.

Facies A4 is formed by limestones (packstones) of foraminifera, mainly miliolids, arranged in tabular to irregular dm- to m- thick beds (Fig. 6d, e). Less abundant are fragments of bivalves, dasycladacean algae and gastropods (Fig. 6f), ostracods and locally, small fragments of crabs. Peloids and mm-sized micritic intraclasts can be abundant locally. Although packstones are dominant, grainstones are locally present. *Thalassinoides* traces also occur.

4.1.2.4.1.2 Facies association B

Facies association B includes four facies (B1 to B4) that, compared with facies association A, are characterized by the presence of charophytes and near-absence of rudists, and presence of fenestral porosity. Locally some irregular, cm-deep paleokarst surfaces appear.

Facies B1 is formed by grainstone-packstone limestones arranged in irregular cm- to dm-thick strata, including foraminifera (mainly miliolids; Fig. 7a), fragmented non-rudist bivalves (and scarce rudists fragments) and dasycladacean algae, and minor proportions of ostracods, gastropods and charophytes. Micritic intraclasts (mm- to cm-sized), peloids, superficial ooids and glauconite are also common. Fenestral porosity is common in both the packstone and grainstone textures (Fig. 7b, c) and cm-thick graded levels and low-angle cross-lamination are locally present.

Facies B2 corresponds to limestones with mudstone-wackestone texture in irregular dm- to m-thick beds. The facies includes few skeletal grains consisting of miliolids, non-rudist bivalve and gastropod bioclasts, ostracods and charophytes, and locally *Favreina*-like coprolites (Fig. 7d). Scarce (mm- to cm- sized) micritic intraclasts and black pebbles are also present. The facies is also characterized by the presence of fenestral porosity and local burrows filled by grainstone sediment similar to that of facies B1.

Facies B3 and B4 includes marls and limestones arranged in dm-thick tabular beds, characterized by the dominance of charophytes (both oogonia and stems) compared to B1 and B2. Facies B3 encompasses marls and limestones (wackestones-packstones) of mainly miliolids and charophytes (Fig. 7e). To a lesser extent non-rudist bivalves, ostracods, gastropods and mm-sized black pebbles and micritic intraclasts are found. Fenestral porosity is scarce. Facies B4 includes marls and limestones (wackestones) dominated by charophytes, big gastropods, and ostracods (Fig. 7f). Fragments of non-rudist bivalves and mm-sized micritic intraclasts are also present. Fenestral porosity is scarce.

4.1.3.4.1.3 Facies association C

Facies association C includes three facies (C1 to C3), all of them showing root traces and fenestral porosity and a low diversity of skeletal grains (charophytes and gastropods).


Facies C1 is formed by dm-thick marls and limestones with wackestone-packstone textures with cm-sized gastropods that appear mostly fragmented. In a lesser proportion are charophytes, cm-sized intraclasts, black pebbles and mm-sized quartz grains (Fig. 8a). Root traces and fenestral porosity are very common.

Facies C2 includes dm- to m-thick marls and dm-thick limestones (mudstone-wackestone) dominated by charophytes and a lesser proportion of gastropods (Fig. 8b). Micritic intraclasts and cm-sized black pebbles are also present. Fenestral porosity (Fig. 8c) and root traces are ubiquitous, and mud-cracks and tepees on top of limestones have been found locally.

Facies C3 corresponds to limestones arranged in tabular dm- to m-thick beds, characterized by the presence of cm-sized black pebbles and intraclasts, and local pisoids. Fossil content is low and consist of commonly fragmented gastropods and few charophytes. The facies ranges from matrix-supported intraclastic-black pebble limestones to intraclastic breccias. The matrix-supported intraclastic-black pebble limestones contains cm-sized rounded black pebbles and angular to sub-angular micritic intraclasts (Fig. 8d, e) floating in a wackestone-packstone matrix that contains abundant mm-sized quartz grains. Fenestral porosity and root traces are frequent. Grain-supported intraclastic breccias locally have accumulations of poorly sorted mm-sized pisoids (Fig. 8f), with concentric, finely laminated cortices. Skeletal fragments (charophytes and gastropods) and small black pebbles and intraclasts form the pisoid nuclei.

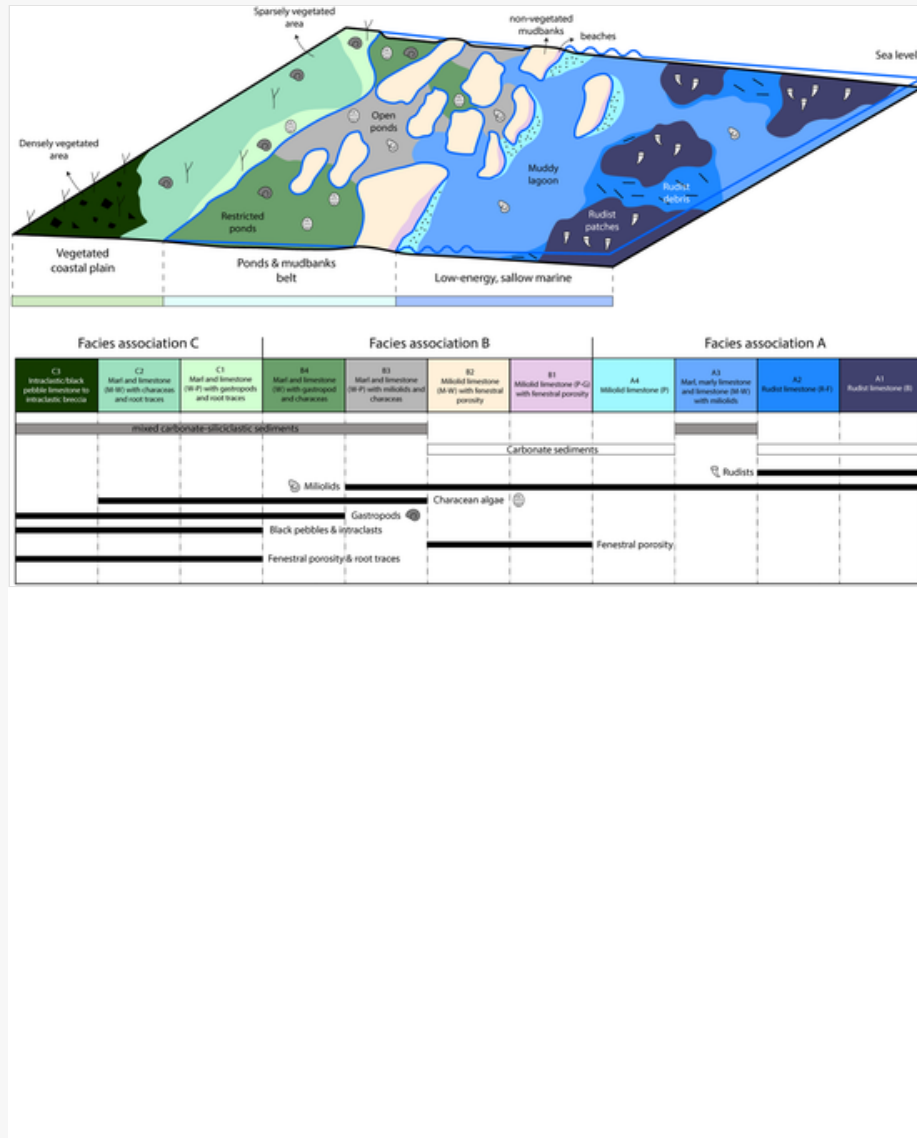
4.2.4.2 Paleoenvironmental interpretation

The sedimentary features of facies and the vertical facies distribution in logs (Fig. 5) are the two main criteria for the interpretation of subenvironments where the La Cañadilla Fm successions accumulated (Fig. 2). Moreover, laterally continuous outcrops were used to check possible lateral facies variations as well as the lateral continuity of carbonate beds and marly intervals. As justified below, facies associations A, B and C, are interpreted respectively as formed in three main subenvironments: a low-energy shallow marine setting, a transitional belt with ponds and emerged mudbanks, and a vegetated coastal plain (Fig. 9).

 Images are optimised for fast web viewing. Click on the image to view the original version.

alt-text: Fig. 9

Fig. 9, **Fig. 9**



Conceptual depositional model for the La Cañadilla Fm indicating the distribution of the key components and structures.

4.2.1.4.2.1 *Low-energy shallow marine lagoon*

Facies association A corresponds to a low-energy, shallow marine area, where skeletal facies (A1 to A4) with bivalves (including rudists, mainly radiolids), foraminifera (mainly miliolids), and dasycladaean algae accumulated (Fig. 4). These facies are usually vertically intercalated (Fig. 5). Rudist boundstones (facies A1) forms discrete (< 1 thick) tabular lithosomes (biostromes) usually vertically associated with facies A2 (rudist rudstone-floatstones). Outcrops conditions allow recognizing the minimum lateral extension of A1 packages of several tens to few hundreds of meters, with local observation of lateral thickness reduction, indicating the possible presence of low-relief bioherms. Rudists usually inhabited lagoons and protected shelves and were also reef/framework bioconstructors (e.g. Kauffman and

Johnson, 1988). The interpretation of these facies as deposited in the seaward part of the low energy lagoon (Fig. 9) is supported by the predominance of radiolitid rudists, the presence of mud-supported textures with miliolids (in both boundstones and rudstone-floatstones), and the poorly rounded rudist shells in the resedimented rudstone-floatstones. Similar radiolitid-dominated facies associated with foraminifera are described in the Upper Cretaceous interior (restricted) platform settings in the Adriatic platform (Moro et al., 2002). The poorly rounded skeletal debris of rudists in the rudstone-floatstone facies A2 were probably generated by bioerosion (Fig. 6B) and physical erosion (e.g. occasional storm events), and were accumulated around the rudists biostromes.

The mud-dominated miliolid-rich marls to limestones, with bivalves and dasycladacean algae (facies A3) is usually related with rudist facies A1 and A2. This facies is interpreted as deposited in a muddy lagoon located landward of the rudist facies (Fig. 9). This landward position agrees with the abundance of miliolids, similar to that described in very shallow marginal marine settings in Upper Cretaceous ramp facies of northern Iberian Basin (Gräfe, 2005). Presence of miliolid-rich marls and marly limestones (not only limestones) in A3 indicates there was episodic input of fine siliciclastics into the lagoon. This condition is not conducive for dasycladacean algae, as they are considered to warm and shallow clear waters (e.g. Aguirre and Riding, 2005; Flügel and Munnecke, 2010). As the dasycladacean algae recorded are broken debris (Fig. 6C), they probably did not inhabit the lagoon, but inhabited more seaward areas from which they were transported. Miliolid-rich packstones (facies A4) usually occurs intercalated in facies A3 (Fig. 5). Both facies have similar components (Fig. 4), but grain-supported texture in A4 points out to deposition under higher-energy conditions than facies A3, probably in shallower (landward) areas of the lagoon, in relation with the emerged mounds of transitional facies (see below). Presence of *Thalassinoides* traces agrees with deposition in lagoon areas (e.g. Knaust et al., 2012).

4.2.2.4.2.2 Ponds and carbonate mudbanks

The transitional belt of ponds and emerged carbonate mudbanks is represented by facies association B. All these facies are skeletal and dominated by non-rudist bivalves, miliolids, characean algae and locally gastropods, thus indicating variable salinity (e.g. Flügel and Munnecke, 2010). Facies B1 consists of grain-supported facies with similar main skeletal grains (miliolids) that facies A4, but is characterized by the widespread presence of fenestral porosity. Well-developed fenestral porosity suggests episodic subaerial exposure (Shinn, 1983; Pratt, 2010). This feature along with the presence of cm-thick graded levels and low-angle cross-lamination suggest deposition in foreshore or beachface with recurrent wave swash, similar to miliolid grainstones described in Barremian-Aptian carbonates in Oman (Pittet et al., 2002). The muddy carbonate facies B2 have skeletal grains (mainly miliolids, but also debris of non-rudist bivalves, gastropod, ostracods and charophytes) and fenestral porosity, and is therefore attributed to episodically exposed carbonate mudbanks (Fig. 9). These facies appear generally as continuous beds. However, outcrops with large lateral continuity allow to observe progressive thickness reduction (and pinching out) of these beds, supporting the possible presence of low-relief carbonate mudbanks. The facies relationship with frequent vertical and lateral abrupt transitions of the pure carbonate facies with evidences of subaerial exposure (B1 and B2) observed at bed scale, point also to the presence of patches of emerged mudbanks and beaches, protecting an inner belt of shallow aqueous ponds where mixed carbonate-siliciclastic facies (B3 and B4) accumulated. Facies B1 and B2 are intercalated between the shallow lagoonal facies A3/A4 and the more restricted facies B3/B4 (Fig. 5). Episodic wave action accumulated miliolid debris in localized beaches from the muddy lagoon (facies A2), in the seaward side of emerged mudbanks (facies B2). Carbonate mudbanks have been described in the geological record, both in land-attached lagoons (e.g. microbial-laminated limestones facies Pérez-Valera and Pérez-López, 2008) and supratidal-intertidal carbonate banks (e.g. algal muddy facies; Sutherland and Henry, 1977). In the studied case, however, there are no evidences of features indicating trapping, binding or baffling of mud, and were probably stabilized by cementation (see discussion). Mud and skeletal grains were sourced from the surrounding ponds and lagoon in both fair-weather and storm conditions, as indicates the skeletal content and the local burrows filled by grainstone sediment of foraminifera and bivalves.

Marls and limestones with very occasional fenestral porosity (facies B3 and B4) accumulated in very shallow ponds or restricted lagoonal areas are interpreted to have experienced subaerial exposure (Fig. 9). These facies are characterized by a lower fossil diversity and presence of charophytes, suggesting a significant fresh water input (e.g. Flügel and Munnecke, 2010) in more proximal areas of the ponds and mudbanks belt. Main skeletal grains in facies B3 (charophytes and miliolids), and facies B4 (charophytes and gastropods, along with ostracods), indicate fluctuations in the salinity, with areas with better connection with normal marine waters (open ponds, facies B3) and restricted areas or ponds with less saline (brackish) waters (facies B4). Similar main skeletal constituents have been described in restricted

or brackish lagoons, ponds and intertidal-to shallow subtidal areas (e.g. Masse et al., 2003; Colombié and Strasser, 2005; Iannace et al., 2014; Nieto et al., 2018).


4.2.3.4.2.3 Vegetated coastal plain

Facies association C is interpreted as deposited above mean sea level, in a low-energy coastal plain, with local presence of submerged fresh-water palustrine to lacustrine areas (Fig. 9). Mixed carbonate-siliciclastic skeletal muddy facies C1 and C2 have evidence of subaerial exposure (root traces, fenestral porosity, local mudcracks), and charophytes and gastropods as main skeletal grains. These features indicate deposition in more landward areas compared to facies association B with which they are vertically related (Fig. 5). In particular, of facies C1 and C2 deposition took place in the coastal plain and submerged ponds in the plain that were colonized by gastropods and charophytes, quite similar to the marginal facies described by Villalba-Breva and Martín-Closas (2013) for the upper Maastrichtian (N Spain). Nevertheless, presence of fragmented charophytes (but not well-preserved thalli) indicates they underwent lateral transport, probably associated with continental runoff events also bringing the muddy siliciclastic sediment (e.g. marls). The near-absence of marine skeletal grains (Fig. 4), and in particular of miliolids typical of the seaward facies reflects this vegetated plain was protected and isolated from the shallow-marine area by the intermediate pond and mudbank belt. Facies C1 and C2 also contain black pebbles and micritic intraclasts sourced from the vegetated areas (e.g. Strasser, 1984), where the intraclastic/breccia facies C3 generated (Fig. 9). Facies C3 ranges from intraclastic-black pebble limestones to intraclastic breccias, and reflect a complex story of reworking in the vegetated plain with mechanical brecciation as a result of root penetration (e.g. Miller et al., 2013).

5.5 Sequence architecture and sedimentary evolution

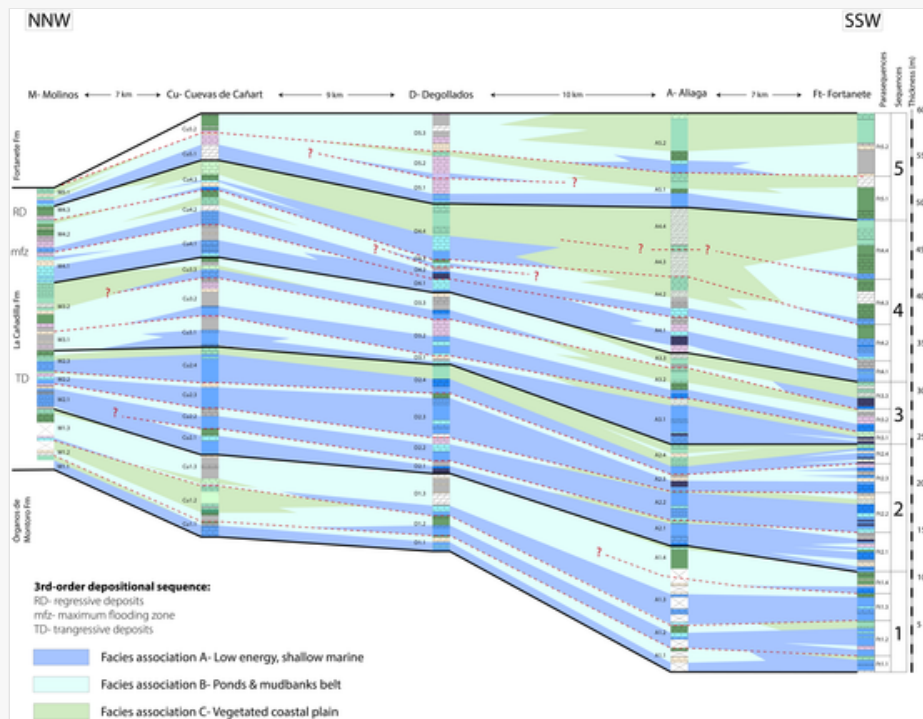
5.1.5.1 Description of sequence stacking

The La Cañadilla Fm represents a third-order depositional sequence, bounded by regional unconformities (Segura et al., 2004). The lower unconformity is the widespread marine flooding surface represented by the onset of the deposition of shallow marine facies association A of La Cañadilla Fm over the brecciated continental facies of the underlying Órganos de Montoro Fm. The upper unconformity is marked by widespread deposition of the continental breccias and lateral counterparts of the Fortanete Fm. At the study area, this depositional sequence shows a well-defined hierarchy of high-frequency sequences, in which smaller (m-thick) parasequences stack in 5 larger-scale sequences (sequences 1 to 5) (Figs. 10 and 11). The procedure for deciphering this hierarchy has followed successive steps: 1) Identification of higher-order sequences (parasequences) in individual logs; 2) Identification of large-scale sequences in individual logs based on long-term vertical trends (See Figs. 5 and 12); 3) Correlation of large-scale sequences along the eastern NNE-SSW trending and western NW-SE trending panels; 4) “Best fit” correlation of sequences, parasequences and facies (Figs. 10 and 11). The lower and upper datum used for the proposed correlation **Q7** are the regional unconformities at the base and top of La Cañadilla Fm. (See Fig. 12.)


 Images are optimised for fast web viewing. Click on the image to view the original version.

alt-text: Fig. 10

~~Fig. 10~~ Fig. 10



Correlation between of the studied logs in the southeastern sector of the studied area (see Fig. 3 for location) showing the distribution of facies associations, sequences and parasequences. See Fig. 5 for the legend of facies and lithology displayed in the stratigraphic logs.


 Images are optimised for fast web viewing. Click on the image to view the original version.

alt-text: Fig. 11

[Fig. 11, Fig. 11](#)

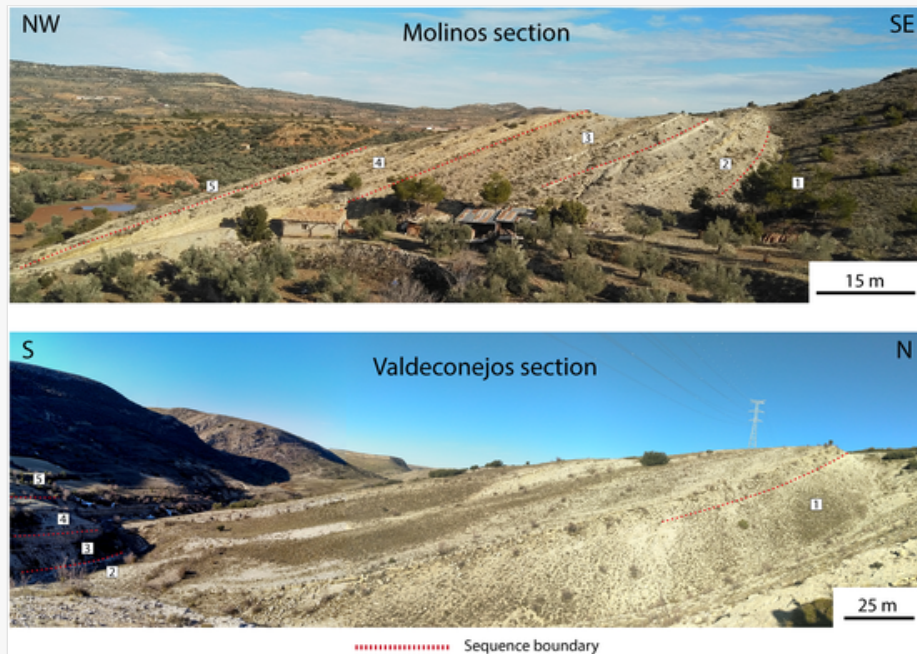


Correlation between the studied logs in the northwestern sector of the studied area (see Fig. 3 for location) showing the distribution of facies associations, sequences and parasequences. See Fig. 5 for the legend of facies and lithology displayed in the stratigraphic logs.

 Images are optimised for fast web viewing. Click on the image to view the original version.


alt-text: Fig. 12

[Fig. 12, Fig. 12](#)



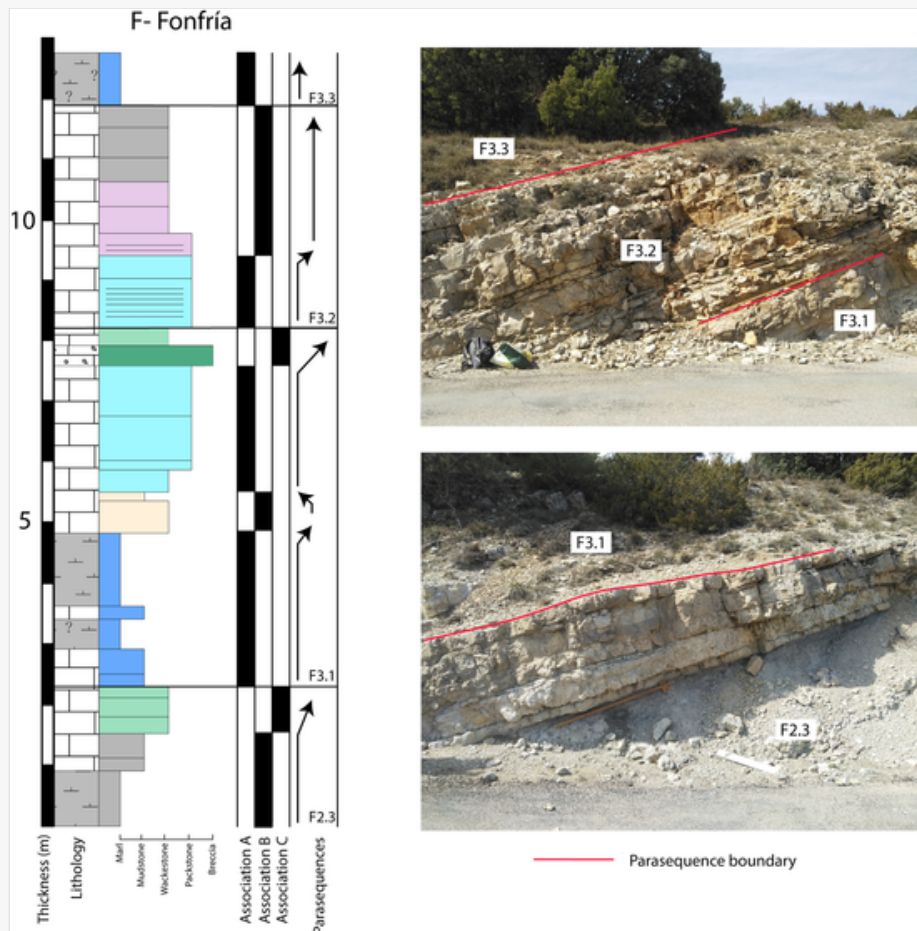
Panoramic field views of the Molinos (M) and Valdeconejos (V) logs indicating the distribution of sequences 1 to 5. Notice that there is not a clearly defined pattern in the overall distribution of the marly dominated levels within the sequence framework (see also [Fig. 16](#)).

The identified higher-order sequences fit the original definition of parasequences (e.g., [Van Wagoner et al., 1988](#); [Catuneanu et al., 2011](#)). They are m-thick (ranging 1.3–7.8-m) shallowing-upward successions, bounded by sharp surfaces that represent an abrupt shift to relative open facies (e.g. marine flooding surfaces). Some parasequences include all the three defined facies associations, passing from low-energy shallow marine facies association A, to ponds and mudbanks belt facies association B, to vegetated coastal plain facies association C, being the upper boundary of the parasequence a shift to shallow marine facies A in the next parasequence (e.g. parasequence Ft3.2 in Fortanete; [Fig. 5](#)). Nevertheless, in most parasequences, shallowing only involves two facies associations, either A–B (e.g., Ft1.3 in Fortanete; F3.2 in Fonfría, [Fig. 13](#)) or B–C (e.g., F1.2 in Fonfría) and locally A–C (e.g., F3.3 in Fonfría). In all the cases, their boundaries are marked by a shift to more seaward facies. In addition, occasionally some parasequences have a deepening-shallowing trend (e.g. Ft1.1 in Fortanete; [Fig. 5](#)) or a more complex vertical stacking of facies, including A–B alternations (e.g. Ft2.3 and Ft2.4 in Fortanete; [Fig. 5](#)). In these cases, flooding surface at the boundary of parasequences is marked by the deposition of the more open rudist facies A1.

 Images are optimised for fast web viewing. Click on the image to view the original version.

alt-text: Fig. 13

[Fig. 13](#), [Fig. 13](#)




Field examples of the parasequences identified in a 13 m-thick interval in Fonfría (F). See Fig. 5 for legend of facies and lithology.

Sequences 1 to 5 were defined in individual logs based on long-term facies trends, in particular the stacking of parasequences in longer-term shallowing-upward sequences (Figs. 10 and 11). Sequences are 6 to 20 m in thickness and formed usually by sets of 3 to 4 parasequences. As a general rule, the lower part of sequences includes shallow marine facies association A, whereas at their upper part facies belonging to ponds and mudbanks belt (facies association B) and vegetated coastal plain (facies association C) predominate. The proposed correlation of sequences and parasequences shown in Figs. 10 and 11 is based on: 1) the similar number of sequences in all logs, which allowed a one-to-one correlation of sequences; 2) the observed lateral continuity of the marine flooding surfaces at the sequence boundaries, indicated by the deposition of shallow marine facies association A over facies associations B or C of the uppermost part of underlying sequence; 3) The quite similar number of parasequences identified in the different logged sections within sequences; and 4) the obtained coherent (best fit) lateral and vertical correlation of their constituent facies associations.

The proposed correlation indicates that parasequences are usually laterally continuous, but locally the number of recorded parasequences decreases in areas of thinner thickness of the sequence and/or when they are dominated by shallowest facies (ponds and mudbanks belt facies association B and vegetated coastal plain facies association C). Sequence 1 (5–12 m thick) consists of 4 parasequences in the southeastern areas (Aliaga and Fortanete; Fig. 10), coincident with the greater thickness of sequence and predominance of shallow marine facies association A. However, towards the north (Fig. 10) and west (Fig. 11) the sequence is thinner and only includes 3 parasequences dominated by facies associations B and C (e.g., Fonfría; Fig. 11). Sequence 2 also presents 4 parasequences in areas of maximum thickness to the southeast (14 m in Fortanete; Fig. 10), but has 3 parasequences in areas of thinner thickness (e.g. Molinos; Fig. 10; Fonfría; Fig. 11). Sequence 3 (6–15 m thick) is formed by 3 shallowing-upward parasequences, except in the northeastern log of Molinos (Fig. 10), where 2 parasequences dominated by facies associations B and C are recorded. Sequence 4 (10–18 m thick) includes 4 parasequences in southern areas where the sequence is thicker (Fortanete and Aliaga; Fig. 10); however, only 3 parasequences are recorded in the northern localities and in the western NW-SE trending panel (Fig. 11), where the sequence is thinner. Sequence 5 (7–11 m thick) includes 2, locally 3 (see log D), parasequences and is dominated by ponds and mudbanks belt facies association B and by vegetated coastal plain association C at their uppermost part (Figs. 10 and 11).

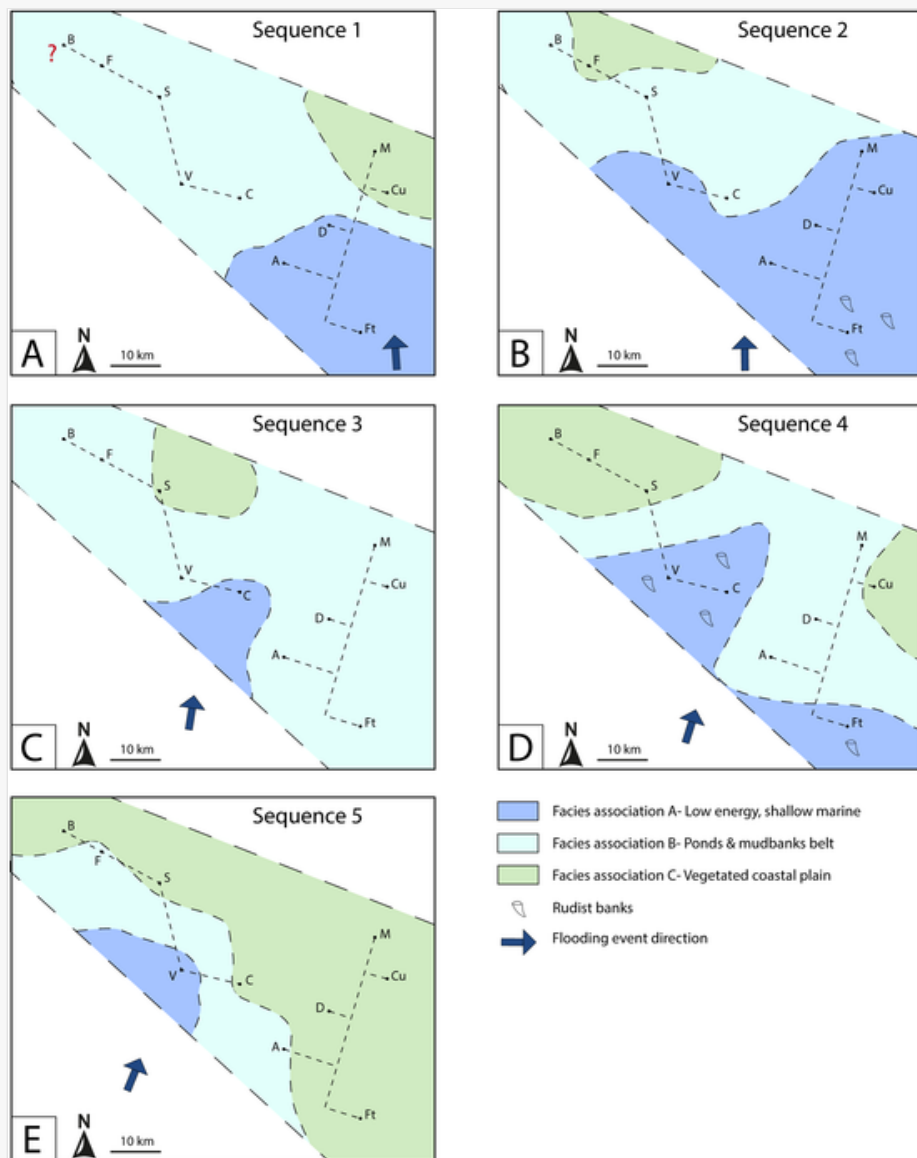
5.2.5.2 Sedimentary evolution

The detailed facies and sequence analyses performed here provide a useful tool for understanding the sedimentary evolution of the La Cañadilla Fm, both at the scale of the entire unit (third-order sequence) and at the more detailed scale of the recorded higher-order sequences 1 to 5. In particular, they provide key criteria to know the relative importance of the transgressive events, either sourced from the Atlantic or from the Tethys realm, that eventually reached the studied marginal area in the South Iberian Ramp (Fig. 1B). Palaeogeographic maps showing the distribution of the three main facies associations for the lower part (second parasequence) of each of the defined sequences 1 to 5 are provided to illustrate the sedimentary evolution of the unit (Fig. 14).

 Images are optimised for fast web viewing. Click on the image to view the original version.

alt-text: Fig. 14

~~Fig. 14~~ [Fig. 14](#)



Facies associations maps reconstructed for sequences 1–5, based in the lateral facies distribution observed in: (A) the middle part of parasequence 1.2; (B) the middle part of parasequence 2.2; (C) the middle part of parasequence 3.2; (D) the middle part of parasequence 4.2; (E) middle part of parasequence 5.1 (see [Figs. 10 and 11](#)). The arrow indicates the main direction of the marine flooding events sourced from the southern Tethyan realm.

In Sequence 1, log correlations indicate that the higher subsidence (greater thickness) and predominance of relative open facies association A locate in southeastern areas ([Figs. 10 and 11](#)). The facies distribution map reveals a more or less W-E trend of facies association boundaries ([Fig. 14A](#)). In particular, the more open rudist-rich facies of the low-energy shallow marine domain located to the southeast, the ponds and mudbanks belt located to the north and

occupying most of the western and central sector, and the vegetated coastal plain was restricted to the northeast area (Molinos, Cuevas de Cañart). This distribution and the larger proportion of the relatively open marine facies association A in the southeastern domain suggest a dominant southern (Tethyan) source for the marine flooding events recorded within parasequences.

Sequence 2 has a significant greater proportion of low-energy shallow marine facies association A in the eastern sector (Fig. 10), including the first record of rudist facies A1 and A2. Facies distribution for the lower part of the sequence (Fig. 14B) clearly reflects the expansion of the low-energy shallow marine domain towards the north compared to sequence 1. An irregular W-E trending of facies associations boundaries can be observed, being the ponds and mudbanks belt and the vegetated coastal plain restricted to the western sector. Therefore, the flooding events recorded at the onset of the parasequences sourced from the south were of such magnitude that they reached the more northeastern areas. Marine flooding events also reached the north-westernmost study area with presence of wedges of low-energy shallow marine facies A in sequence 2 in the Bea log (Fig. 11).

Sequence 3 has a widespread deposition of low-energy shallow lagoonal facies A within the lower parts of its parasequences. These are more extensive than in sequence 2 in the western sector and include the first record of rudist facies in westernmost logs (Fig. 11). These marine flooding events are followed by sharp shallowing to facies associations B and C within the parasequences (Figs. 10 and 11). Areal facies distribution for the lower part of the sequence (Fig. 14C) indicates that most of the study area was occupied by the ponds and mudbanks belt. In addition, there is a more irregular trend of facies associations boundaries, with a subtle change to a NW-SE trend compared to W-E trend of sequences 1 and 2. Taking into account the distribution of the wedges of low-energy shallow marine facies A (Figs. 10 and 11), the marine flooding events probably had a dominant southern (Tethyan) source.

Log correlations in sequence 4 reveal that low energy shallow marine facies association A is present in almost all parasequences, although there is a significant increase in the proportion of facies associations B and C compared to sequence 3 (Figs. 10 and 11). In particular, shallow marine facies A including rudist facies A1 and A2 predominate in the sequence in western sector (see V and C logs in Fig. 11). Facies distribution for the lower part of the sequence (Fig. 14D) indicates the presence of this low-energy shallow marine domain at Valdeconejos-Cirugeda area and also to the southeast (see F log in Fig. 11). The significant increase in the proportion of facies associations B and C compared to previous sequences involves the presence of two areas of vegetated coastal plains to the northeast and to the northwest. The irregular NW-SE trend of facies associations boundaries is greater than in sequence 3. The reconstructed lateral and vertical facies distribution (with wedges of marine facies A both in the west and east) indicate that marine flooding events were probably sourced from southern areas.

Sequence 5 includes minor proportion of shallow marine facies association A, being rudist facies absent. This fact and the predominance of facies belonging to pond and mud banks belt and vegetated coastal plain is clearly reflected in the facies distribution map (Fig. 14E). Most of the studied area is occupied by vegetated coastal plain, being ponds and mudbanks belt and shallow marine domains located to the western sector (see log V in Fig. 14E), which were most probably sourced from the southern Tethyan realm.


The evolution of sedimentary domains during the development of sequences 1 to 5 allows to locate the maximum flooding zone of La Cañadilla Fm at the lower part of sequence 4, based on the presence of facies association A from sequence 1 to lower part of sequence 4, and predominance of facies associations B and C above (Figs. 10 and 11). Sequences 1 to lower part of sequence 4 would therefore represent the transgressive deposits of the third-order sequence, characterized by an upward increase of low energy shallow marine facies association A, being the maximum expansion of the relatively more open rudist facies A1 and A2 recorded at the lower part of sequence 4. Upwards, the upper part of sequence 4 and the entire sequence 5 would correspond to the regressive deposits, as there is a reduction of the proportion of low energy shallow marine facies and a clear predominance of facies associations B (ponds and mudbanks belt) and C (vegetated coastal plain).

The sedimentary evolution deciphered in the studied successions of South Iberian Ramp, and in particular, the dominant influence of Tethyan sourced flooding events (Fig. 14), provide more precision to previous palaeogeographic data for the Upper Cretaceous successions in the Iberian Basin (Alonso et al., 1993; Segura et al., 2004; Gil et al., 2004; Martín-Chivelet et al., 2019). According to Alonso et al. (1993), the transgressive events sourced from the Atlantic realm were dominant in the Iberian Basin from Albian to the end of the Cretaceous. However, Segura et al. (2004) indicated the importance of Tethys transgressions during late Santonian-early Campanian, as it has been reconstructed

in the present study. Moreover, these authors also suggest a progressive migration of the transgressive pulses from the southeast to the southwest during sedimentation. This change in the direction of flooding sources, along with the change in the orientation of facies belt boundaries has been also deciphered in detail in the present study.

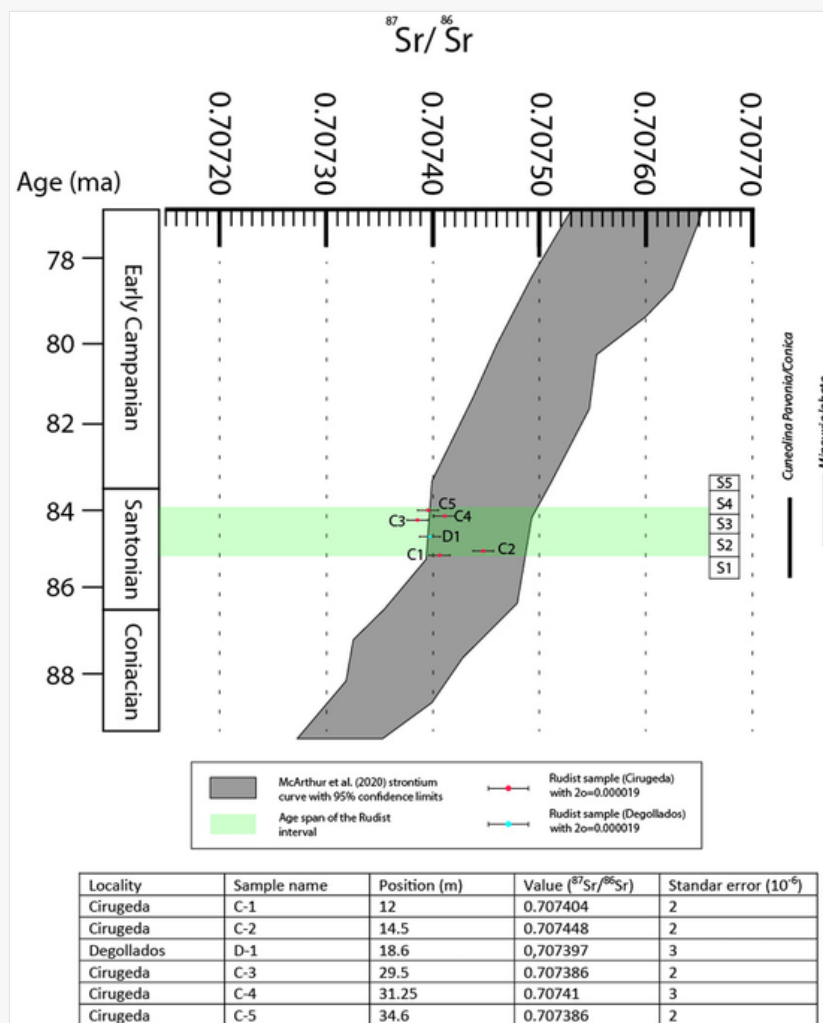
6.6 Age calibration of La Cañadilla Fm

The latest Santonian-early Campanian age for La Cañadilla Fm previously proposed by Segura et al. (2004) and García et al. (2004) fits well with the benthic foraminifera association identified here in La Cañadilla Fm. This association includes: *Valvulamina picardi*, *Quinqueloculina sp.*, *Textularia sp.*, *Vidalina hispánica*, *Stensionina surrentina*, *Ataxophragmium sp.*, *Idalina antiqua*, *Minouxia lobata*, *Peneroplis giganteus*, *Pseudolituonella mariae*, *Cuneolina conica*, *Cuneolina pavonia*, *Ophthalmidium sp.* and *Rotalina cayeuxi* (for the biostratigraphic ranges of this benthic foraminifera association see Filkorn and Scott, 2011; Frijia et al., 2015; Solak et al., 2017). Of particular interest is the presence of *Cuneolina pavonia* and *Cuneolina conica* up to the upper part of S4 in La Cañadilla Fm (Fig. 15). These foraminifera are reported in the European Tethys to disappear after the Santonian (Filkorn and Scott, 2011), probably indicating that S5 would represent the basal Campanian. Also of interest is *Minouxia lobata* that is reported by Velić (2007) to have an age range from middle Santonian to Campanian. In La Cañadilla Fm *Minouxia lobata* is recognised upwards from S2, suggesting that the lower part of the unit should be not older than middle Santonian (Fig. 15). On the other hand, the rudist association identified by Astre (1929) in the La Cañadilla Fm, with *Praeradiolites toucasi*, *Praeradiolites plicatus*, *Radiolites mammillaris*, *Radiolites galloprovincialis*, *Biradiolites angulosissimus*, *Biradiolites retrolatus* and *Radiolites hispanicus* has been described in other middle Santonian-early Campanian successions (Alegret and Aurell, 1998; Vicens et al., 1998).

 Images are optimised for fast web viewing. Click on the image to view the original version.

alt-text: Fig. 15

[Fig. 15](#)



Age calibration proposed for La Cañadilla Fm on the basis of stable isotopic data ($^{87}\text{Sr}/^{86}\text{Sr}$) obtained from six well-preserved rudist shells, and its comparison with the global curve for the Upper Cretaceous after [McArthur et al. \(2020\)](#). A table showing location, name, stratigraphic position, value and standard error of the samples is also displayed. The stratigraphic distribution within the La Cañadilla Fm of the two benthic foraminifera with biostratigraphic relevance is also indicated (see text for explanation).

In order to constrain the age of La Cañadilla Fm, $^{87}\text{Sr}/^{86}\text{Sr}$ isotope data from six well-preserved rudist shells were obtained from S2, S3 and lower S4 in Cirugeda and Degollados logs ([Fig. 15](#)). The mean value of $^{87}\text{Sr}/^{86}\text{Sr}$ obtained is 0.710245 ± 0.000019 . The specific data of the samples have been plotted on the [McArthur et al. \(2020\)](#) strontium 87/86 curve. The obtained strontium data give a wide age range, from Coniacian to mid-early Campanian. However, taking into account the biostratigraphic constraints provided by the benthic foraminifera and rudist association, the best fit approximation indicates that the most probable age of La Cañadilla Fm is middle Santonian-earliest Campanian, with the Santonian-Campanian boundary located around the upper part of Sequence 4.

7.7 Discussion

7.1.7.1 La Cañadilla Fm: a possible ancient analogue of the Ten Thousand Island of Florida

La Cañadilla Fm shows a complex set of interfingering facies developed in a low-energy and low-gradient shallow marine to coastal environment, including three main subenvironments: a low energy shallow marine lagoon inhabited mainly by radiolitid rudists and miliolids, a transitional belt with a patchy distribution of ponds and mudbanks colonized by miliolids, and by charophytes and gastropods, and a vegetated coastal plain with high freshwater influence, allowing the widespread colonization by plants, gastropods and charophytes. Input of fine siliciclastics (giving rise to marls and marly limestones) was recorded episodically in the three subenvironments, but pure carbonate sediments mainly accumulated in the seaward part of the shallow marine area (rudist colonization area) and within mudbanks ([Fig. 9](#)).


Vertical and lateral distribution suggests a heterogeneous or a mosaic-like facies arrangement in the reconstructed coastal carbonate mud-plain environment. Absence of any evidence of common tidal flat structures such as tidal channels or tide-derived laminations could indicate a low energy wave regimen and an attenuated tidal range in this low-gradient plain. A very low (or even negligible) tidal range in the marginal areas of the South Iberian Ramp studied here (see [Fig. 1B](#)) would be explained by the tidal dumping by friction with the shallow bottom in the interior areas of the Iberian seaway, that would inhibit tidal exchange, similar to that which has been recorded in the interior areas of the Florida Bay (e.g. [Reading, 1978](#); [Wang et al., 1994](#)) or has been interpreted in the Upper Jurassic Iberian carbonate ramps (e.g. [Bádenas and Aurell, 2001](#)). Fair weather wave base is also assumed to be very shallow, allowing the sedimentation of shallow-water mud-supported facies. The presence of grain-supported skeletal facies is therefore interpreted as originated mostly by the episodic action of storm-induced currents and waves.


A possible modern analogue of the complex system represented by the La Cañadilla Fm is found in the southern Florida coast, including the Florida Bay or the Ten Thousand Island system. There the low-energy wave regime (mean annual wave height of 10–25 cm; [Tanner, 1960](#)), and attenuated tidal range (1.3 m; [Davis et al., 1992](#)) is likely representative of conditions that prevailed in some Upper Cretaceous epeiric platforms and coastal plains ([Lacovara et al., 2003](#)). The Ten Thousand Island system has a complex transitional belt between the shallow marine and coastal areas, which includes a mosaic of islands and restricted ponds with reduced tidal circulation ([Shier, 1969](#)). There, the islands are covered by vegetation dominated by a variety of mangrove-associates, which greatly influence the trapping of sediment. However, this differs with the mudbanks (facies B2) of La Cañadilla Fm, which lack evidence of vegetation cover (e.g. root bioturbation). In the shallow restricted lagoon of the Florida Bay, carbonate mudbanks do not have extensive supratidal vegetation (e.g. [Bosence, 1995](#)). The difficulty of understanding the interaction between organic and inorganic processes challenges their interpretation, and there has been discussion whether these mounds may have originated by in situ carbonate production, or by hydrodynamic and physical processes or a combination of both (e.g., [Heckel, 1974](#); [Bosence and Waltham, 1990](#); [Wanless et al., 1995](#); [Riding, 2002](#)). In the case of mudbanks of La Cañadilla Fm, symsedimentary cementation of muddy sediments (as indicate the presence of fenestral porosity) could have been a key process for stabilization of the mudbanks. It has to be noted that the search for Florida Bay analogues in ancient rocks is hampered by the low relief on the mudbanks ([Enos and Samankassou, 2022](#)). The slopes on the flanks of the mounds are generally less than $\leq 1^\circ$, even in the narrow banks of the eastern Bay ([Enos and Perkins, 1979](#)). Such gentle slope angles are hard to be detected in outcrop. However, lateral continuity of beds in some of the studied outcrops allowed to recognize variations in bed thickness supporting the presence of mudbanks with low depositional relief.


Low-energy and low tidal regime for La Cañadilla Fm can be deduced by the predominance of mud-supported textures, the absence of tidal channels facies and tidal-related lamination, and the very local presence (e.g. low-angle cross-lamination) of sedimentary structures related to waves and/or currents. Despite low-energy, episodic wave or current action (including storms) is recorded in the Ten Thousand Island system and Florida Bay mudbanks, both accumulating grain-supported textures or contributing to the physical erosion of the mudbanks (Enos and Perkins, 1979 ; Bosence, 1989; Enos, 1989; Wingard et al., 2020). This episodic influence of high-energy process is also recorded in La Cañadilla Fm by the presence of skeletal packstone/grainstone facies, which are interpreted to be deposited in the seaward side of the mudbanks (B1 and A4: Fig. 9). These grain-supported accumulations could contribute to the preservation of mudbanks, at least in those located in the seaward side of the ponds and mudbanks belt.

The rock record presents a variety of potential ancient counterparts for Ten Thousand Island system and Florida Bay. From these, the shallow marine lower Devonian Manlius Formation from New York was related to small fluctuations in water level due to lunar tides, storms or seasonal climatic variation along with local differences in sediment accumulation and erosion (Laporte, 1967). This led to the advancing and retreating of three facies groups (subtidal, intertidal and supratidal) forming a complex facies mosaic that is compared to the “facies mosaic” of Florida (Laporte, 1967). Eocene mudbanks of the Pyrenean foreland basin (Spain) seem to be generated as biotrital grains physically deposited and present the same environmental setting, size and composition of those located in the Florida Bay (Taberner and Bosence, 1995). Middle Triassic carbonates in southern Spain present mudbanks formed by fine and cohesive-laminated sediment in a high energy context that is compared to the mudbank sediments from Florida (Pérez-Valera and Pérez-López, 2008). Lofer cyclothems of the Alpine Upper Triassic have also many features in common with Holocene sediments of Florida Bay. In this case, lateral discontinuity and thickness variations indicate syndepositional relief, possibly in the form of mudbanks (Enos and Samankassou, 2022). The example of La Cañadilla Fm shown here, add a new example of mosaic of facies, in which carbonate mudbanks, were probably syndepositional-cemented and formed a key belt protecting the interior ponds and coastal plain.

7.2.7.2 Possible orbital control of sequences and parasequences

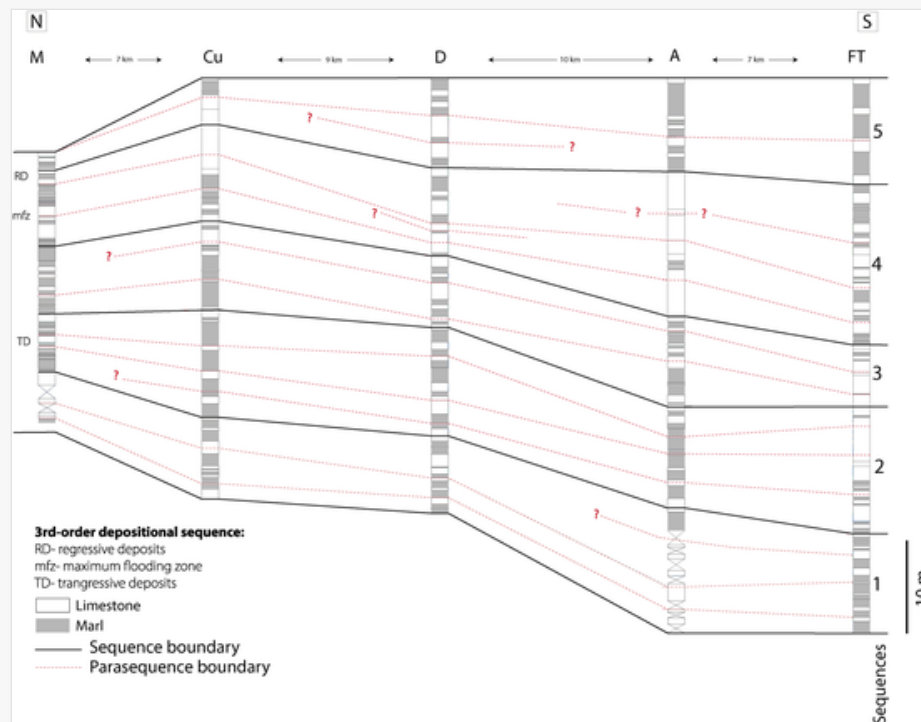
The La Cañadilla Fm has a well-defined stacking of sequences and parasequences. The lateral continuity of sequences 1 to 5 along the 40 km ~~✖~~  80 km wide studied area suggests allogenic processes (at least at basin scale) controlling their formation. Other alternative explanation, like pulsed, tectonic control for the creation and filling of accommodation space (e.g. Bosence et al., 2009) is not supported by data. The number of parasequences per section is kept relatively constant, there is no significant thickness variations of parasequences and sequences both at outcrop (local) and regional scale, and the cycle type is quite homogeneous and with a well-defined stacking pattern.

The usual presence of 3 to 4 parasequences within sequences reflects a possible allogenic (periodic) factor in their generation. The age calibration of La Cañadilla Fm give additional information to relate the identified sequences and parasequences to any of the known orbital cycles. In particular, the combined datation using strontium and bisotratigraphic data permit to estimate, according to the geological time scale (e.g., McArthur et al., 2020) a duration of about 2.5 My for the whole duration of La Cañadilla Fm (Fig. 15). Assuming a similar duration for the identified sequences, each of the 5 sequences 1 to 5 would have a c.500 ky duration and could be tentatively assigned to the long-orbital eccentricity cycle. In turn, the parasequences would fit the short-eccentricity cycle, considering the observed number of 3 ~~✖~~  4 parasequences within sequences 1 to 5. It may be therefore suggested that the orbital variation of the eccentricity cycle resulted in climate-driven low-amplitude sea-level oscillations that generated the sequential architecture observed in La Cañadilla Fm.

Orbitally-driven climate changes may result in a sequential arrangement indicating a cyclic carbonate-siliciclastic  sedimentation in shallow marine environments (e.g. Val et al., 2019). However, when analysing the marl-limestone vertical evolution of La Cañadilla Fm, there is no clear pattern suggesting a periodic siliciclastic input over time. Fig. 16 shows a simplified version of the southeastern correlation panel highlighting the distribution of marls and limestones. There is no estimable distribution-pattern at parasequence, sequence or third-order sequence scale. This suggests that the lithological alternation of marls and limestones in La Cañadilla Fm is not related the climate changes formed in tune with the eccentricity cycles but to local basinal factors or other stationary shorter cycles.

alt-text: Fig. 16

Fig. 16. Fig. 16



Simplified version of the southeastern correlation panel (see Fig. 10) showing the vertical distribution of the alternation between marls and limestones of La Cañadilla Fm. Notice that there is not a clearly defined pattern in the overall distribution of the marly dominated levels within the sequence framework.

A major feature of the Cretaceous sedimentary record is cyclic bedding rhythms that display periodicities in the Milankovitch frequency band (e.g., Dean et al., 1984; Kuhnt et al., 2001). A well-documented example is the upper Turonian to lower Coniacian shallow marine carbonate succession analysed by Gil et al. (2009) in the northern Castilian Ramp. This succession is subdivided in meter-scale parasequences and parasequence sets, which have interpreted to be related to sea level oscillations formed probably in tune with the short- and long-term eccentricity orbital cycles. This imprint of orbital cycles has been also recorded in other Upper Cretaceous successions of the Tethys realm. Le Goff et al. (2015) studied the carbonates of the southeastern Apulian Platform on the Albanian side with sedimentological features similar to La Cañadilla Fm (rudist-dominated subtidal areas, and breccias and fenestral mudstones in inter-supratidal areas) and describe meter-thick shallowing cycles controlled by sea-level fluctuations, which are tentatively related to orbital processes. Carannante et al. (2000) describes the lower Campanian carbonates in the Sorrento Peninsula (Italy) as representing deposition in intertidal and subtidal areas (also including foraminifera and rudists) highly influenced by storms that stack in dm-thick shallowing cycles. The cycles are also interpreted as a result of relative sea-level oscillations, however their relation to Milankovitch cycles is debated. Simone et al. (2003) study Coniacian-lower Campanian carbonate shelves with mainly radiolitic rudists of central-southern Italy and describe meter-thick shallowing up parasequences, although without inferring an orbital origin but a relation with submarine erosion and high-energy events.

Outside the Tethys realm there are also studies relating the stacking of high-frequency sequences or cycles and other sedimentary (e.g. chemostratigraphic) trends with possible climate orbital-driven changes, both in marine and continental successions. Al-Husseini (2018) measure $\delta^{13}\text{C}$ records in several marine successions of the Albian-Lower Campanian of Southern England and found a link between $\delta^{13}\text{C}$ events and orbital forcing cycles, some of which have been also recognized in Europe (Uličný et al., 2014), Japan (Takashima et al., 2010), North America (Joo and Sageman, 2014) and Tanzania (Wendler and Wendler, 2016). Liu (2007) establishes a stacking pattern of eccentricity cycles in the cm- to m-thick marine chalk-marl pairs of the Santonian-Campanian in the northeastern Gulf of Mexico. Wu et al. (2014) perform the cyclostratigraphic analysis of Santonian-Danian continental strata (Songliao Basin, northeastern China), describing eccentricity, obliquity and precession cycles. Cenomanian units of the Starigrad

Formation (Hvar, Croatia) studied by [Diedrich et al. \(2011\)](#) also presents shallow marine/lagoonal facies arranged in shallowing upwards parasequences dm- to m-thick. The maximum flooding surface is also located at the base of massive rudist banks, despite the orbital origin of this cyclicity is not studied, the transgressive event affecting these units fits with the Upper Cenomanian event defined by [Segura et al. \(2004\)](#) in the Iberian Basin and could support a possible regional extent of these events.

Despite sequences and parasequences of the third-order sequence of La Cañadilla Fm are thought to be related with low amplitude sea level oscillations driven by eccentricity (400 ky and 100 ky) cycles, other factors also influenced their preservation in the sedimentary record. In particular, the 1/4 figure for sequences/parasequences is not always present, as the number of parasequences usually laterally decreases in less subsident areas and/or in the intervals dominated by the shallowest facies association C ([Figs. 10 and 11](#)). This fact fits the trend observed in similar 100 ky-sequences within 400 ky-sequences in Jurassic marine successions, where in areas of less subsidence the number of 100-ky sequences is minor, so that some 100-ky sequences did not accumulate or are amalgamated ([Bádenas et al., 2010](#); [Sevillano et al., 2021](#)). In the case studied here, log correlation points out to a possible merging or amalgamation of 100 ky-parasequences in less subsident areas. Presence of 2 or 3 parasequences in sequence 5 dominated by shallowest facies (ponds and mudbanks belt facies association B and vegetated coastal plain facies association C) also conforms to the model of [Bádenas and Aurell \(2018\)](#) of lower preservation potential of 100 ky-related sequences in shallow settings with low accumulation rates, due to the combination of low accommodation and internal factors of sediment production and erosion/accumulation.

8.8 Conclusions

The shallow marine-coastal carbonate-mud dominated succession of La Cañadilla Fm deposited during the Late Cretaceous in the northeastern marginal areas of the Southern Iberian Ramp (Iberian Basin, Spain) has been studied here to characterize facies distribution and sequential architecture. A total of 11 facies have been differentiated, grouped in three facies associations related to the three differentiated belts: (1) a low energy shallow marine lagoon mainly colonized by radiolitic rudists and miliolids; (2) a transitional belt with a patchy distribution of ponds and carbonate mudbanks with variable proportion of miliolids, charophytes and gastropods; (3) a vegetated coastal plain with high freshwater influence, allowing the widespread colonization by plants, gastropods and charophytes.

The complexity of the transitional belt with mudbanks and ponds resulted in mosaic facies distribution. This belt compares to modern analogues such as the Florida Bay or the Ten Thousand Island system, with shallow marine and coastal areas including a mosaic of emerged islands and restricted ponds with reduced tidal circulation. Tidal range and normal wave base were also negligible during the sedimentation of La Cañadilla Fm, favouring the sedimentation of mud-supported facies. The local presence of grain-supported skeletal facies is interpreted as originated mostly by the episodic action of storm-induced currents and waves. Synsedimentary cementation of muddy sediments seem to be the key factor controlling the stabilization of the mudbanks in La Cañadilla Fm. As in Florida, grain-supported accumulations in the seaward side of the transitional belt could also contribute to the preservation of mudbanks.

New strontium isotopic data constrained by the distribution of some key benthic foraminifera (*Minouxia Lobata*, *Cuneolina Pavonia* and *Cuneolina Conica*) indicates a middle Santonian to early Campanian age for La Cañadilla Fm. This unit shows a well-defined hierarchy of m-thick parasequences stacking in 5 larger-scale sequences. A possible orbital origin for the reconstructed sequential architecture is suggested based on the total duration of La Cañadilla Fm and the number of parasequences. Sequences would fit in the long-term eccentricity orbital cycles (c.400 ky), while parasequences would fit in the short-term (c.100 ky). The orbital variation resulted in climate-driven low-amplitude sea level oscillations that caused the episodic flooding of the low-gradient carbonate ramp. These flooding events were mostly sourced from Tethyan realm. Therefore, the sedimentary model and sequential architecture of La Cañadilla Fm can help in better understanding of both sedimentation in the eastern Iberian Basin and the impact of orbital cyclicity during the Late Cretaceous.

Q10 Uncited reference

~~Tedesco and Wanless, 1990~~


Declaration of competing interest

The authors declare that they have no known competing financial interests or personal relationships that could have appeared to influence the work reported in this paper.

Acknowledgments

This paper was funded by projects CGL [2017-85038-P](#) and Group E18 (Aragosaurus: Recursos Geológicos y Paleambientales) subsidized by the [Spanish Ministry of Science and Innovation](#), the [European Regional Development Fund](#) and the [Government of Aragón](#). The research of Diego Torromé is funded by a [DGA Grant](#) (Aragón department of science, university, and society of knowledge). The authors would like to acknowledge the use of the Servicio General de Apoyo a la Investigación-SAI, Universidad de Zaragoza. We are grateful for the revision done by Michele Morsilli, an anonymous reviewer and the Editor-in-Chief Massimo Moretti which highly improved the original version **Q11** of the manuscript.

References

 The corrections made in this section will be reviewed and approved by a journal production editor. The newly added/removed references and its citations will be reordered and rearranged by the production team.

Aguirre, J., Riding, R., 2005. Dasycladalean algal biodiversity compared with global variations in temperature and sea level over the past 350 Myr. *Palaios* 20, 581–588.

Alegret, L., Aurell, M., 1998. Contribución a la taxonomía y bioestratigrafía de los rudistas del Cretácico superior en el Prepirineo aragonés. pp. 29–43 (in spanish with english abstract).

Al-Husseini, M., 2018. Orbital-forcing of Cenomanian–Santonian glacio-eustasy. In: *Orbital Scale.net*.

Almunia, A., Arqued, V., Meléndez, A., 1985. Características sedimentarias durante el ciclo Senosiense en el Maestrazgo. *Trabajos de Geología* 15, 159–169 (in spanish, with english abstract).

Alonso, A., Floquet, M., Mas, [J.-R.J.R.](#), y Meléndez, A., 1993. Late Cretaceous platforms: origin and evolution, Iberian Range, Spain. In: Simo, J.A.T., Scott, R.W., Masse, J.P. (Eds.), *Cretaceous Carbonate Platforms*. In: *American Association of Petroleum Geologists*, 56. pp. 297–313.

Arche, A., López-Gómez, J., 1996. Origin of the Permian-Triassic Iberian basin, central-eastern Spain. *Tectonophysics* 266, 443–464.

Astre, G., 1929. La faune des Radiolitidés de Fortanete. *Bulletin de la Société Géologique de France* 4, 227–234 (in french).

Aurell, M., Fregenal-Martínez, M., Bádenas, B., Muñoz-García, [M.-B.M.B.](#), Élez, J., Meléndez, N., De Santisteban, C., 2019. Middle Jurassic–Early Cretaceous tectono-sedimentary evolution of the southwestern Iberian Basin (central Spain): Major palaeogeographical changes in the geotectonic framework of the Western Tethys. *Earth-Science Reviews* 199, 102–983.

Baceta, J., Pujalte, V., Serra-Kiel, J., Robador, A., Orue-Etxebarria, X., Vera, J., 2004. El Maastrichtense final, Paleoceno e Ilerdiense inferior de la Cordillera Pirenaica. In: Vera, [J.-A.J.A.](#) (Ed.), *Geología de España*. Sociedad Geológica de España and Instituto Geológico y Minero de España, Madrid, pp. 308–313 (in spanish).

Bádenas, B., Aurell, M., 2001. Proximal–distal facies relationships and sedimentary processes in a storm dominated carbonate ramp (Kimmeridgian, northwest of the Iberian Ranges, Spain). *Sedimentary Geology*

Bádenas, B., Aurell, M., 2018. The down-dip preferential sequence record of orbital cycles in greenhouse carbonate ramps: examples from the Jurassic of the Iberian Basin (NE Spain). *Stratigraphy & Timescales* 3, 285–325.

Bádenas, B., Aurell, M., Bosence, D., 2010. Continuity and facies heterogeneities of shallow carbonate ramp cycles (Sinemurian, Lower Jurassic, North-east Spain). *Sedimentology* 57, 1021–1048.

Bosence, D., 1989. Surface sublittoral sediments of Florida Bay. *Bulletin of Marine Science* 44, 434–453.

Bosence, D., 1995. ~~Anatomy of a Recent biotrital mud-mound from Florida Bay, USA~~Anatomy of a recent biotrital mud-mound from Florida Bay, USA. In: Monty, C.L.V., Bosence, D.W.J., Bridges, P.H., Pratt, B.R. (Eds.), *Carbonate Mud-mounds: Their Origin and Evolution*. In: Int. Assoc. Sedimentol. Spec. Publ. 23. Blackwell, Oxford, UK, pp. 475–494.

Bosence, D., Waltham, D., 1990. Computer modeling the internal architecture of carbonate platforms. *Geology* 18, 26–30.

Bosence, D., Procter, E., Aurell, M., Bel Kahla, A., Boudagher-Fadel, M., Casaglia, F., Rey, J., 2009. A dominant tectonic signal in high-frequency, peritidal carbonate cycles? A regional analysis of Liassic platforms from western Tethys. *Journal of Sedimentary Research* 79, 389–415.

Canerot, J., Cugny, P., Pardo, G., Salas, R., Villena, J., 1982. Ibérica Central-Maestrazgo. In: Universidad Complutense de Madrid and CSIC (Ed.), *El Cretácico de España*. Editorial Universidad Complutense de Madrid, Madrid, pp. 273–344 (in spanish).

Carannante, G., Ruberti, D., Sirna, M., 2000. Upper Cretaceous ramp limestones from the Sorrento Peninsula (southern Apennines, Italy): micro- and macrofossil associations and their significance in the depositional sequences. *Sedimentary Geology* 132, 89–123. doi:10.1016/S0037-0738(00)00004-X.

Casas, ~~A. M. A. M.~~, Casas, A., Pérez, A., Tena, S., Barrier, L., Gapais, D., Nalpas, T., 2000. Syn-tectonic sedimentation and thrust-and-fold kinematics at the intra-mountain Montalbán Basin (northern Iberian Chain, Spain). *Geodinamica Acta* 13, 1–17.

Catuneanu, O., Galloway, ~~W. E. W. E.~~, Kendall, C., Miall, ~~A. D. A. D.~~, Posamentier, ~~H. W. H. W.~~, Strasser, A., Tucker, M., 2011. Sequence stratigraphy: methodology and nomenclature. *Newsletters on Stratigraphy* 44, 173–245.

Colombié, C., Strasser, A., 2005. Facies, cycles, and controls on the evolution of a keep-up carbonate platform (Kimmeridgian, Swiss Jura). *Sedimentology* 52, 1207–1227.

Davis, R.A., Jr., Hine, A.C., Shinn, E.A., 1992. Holocene coastal development on the Florida peninsula. In: Fletcher, C.H., Wehmiller, J.F. (Eds.), *Quaternary Coasts of the United States: Marine and Lacustrine Systems*. In: SEPM Spec. Publ. 48. pp. 193–212 (Oklahoma).

Dean, W., Arthur, M., Stow, D., Hay, ~~W. W. W. W.~~, 1984. ~~Origin and geochemistry of Cretaceous deep-sea black shales and multicolored claystones, with emphasis on DSDP Site 530, southern Angola Basin~~Origin and geochemistry of cretaceous deep-sea black shales and multicolored claystones, with emphasis on DSDP Site 530, southern Angola Basin. In: Sibuet, J.C. (Ed.), *Initial Reports of the Deep Sea Drilling Project*, 75. U.S. Government Printing Office, Washington D.C., pp. 819–844.

Dercourt, J., Gaetani, M., Vrielynck, B., Barrier, E., Biju-Duval, B., Brunet, M., Sandulescu, M., 2000. ~~Peri-Tethys palaeogeographical atlas 2000~~[Peri-Tethys Palaeogeographical Atlas 2000](#). Université Pierre et Marie Curie, Paris.

Diedrich, C., Caldwell, ~~M. W.~~[M.W.](#), Gingras, M., 2011. ~~High-resolution stratigraphy and palaeoenvironments of the intertidal flats to lagoons of the Cenomanian (Upper Cretaceous) of Hvar Island, Croatia, on the Adriatic Carbonate Platform~~[High-resolution stratigraphy and palaeoenvironments of the intertidal flats to lagoons of the Cenomanian \(Upper cretaceous\) of Hvar Island, Croatia, on the Adriatic Carbonate Platform](#). Carbonates and Evaporites 26, 381–399. doi:10.1007/s13146-011-0073-2.

Dunham, ~~R. J.~~[R.J.](#), 1962. Classification of carbonate rocks according to depositional textures. American Association of Petroleum Geologists Bulletin 1, 108–121.

Embry, ~~A. F.~~[A.F.](#), Klován, J., 1971. A late Devonian reef tract on northeastern Banks Island, NWT. Bulletin of Canadian Petroleum Geology 19, 730–781.

Enos, P., 1989. Islands in the bay—a key habitat of Florida Bay. Bulletin of Marine Science 44, 365–386.

Enos, P., Perkins, R., 1979. Evolution of Florida Bay from island stratigraphy. Geological Society of America Bulletin 90, 59–83.

Enos, P., Samankassou, E., 2022. Florida Bay: modern analogue for Lofer cyclothems? Sedimentology 69, 254–281.

Feuillée, P., 1967. Le Cénomanien des Pyrénées basques aux Asturies: essai d'analyse stratigraphique. In: ~~Claude-Bernard (Ed.), Mém. Soc. Géol. Fr~~[Mémoires de la Société géologique de France](#), 46. ~~Société géologique de France-p.~~, p. 343 (in french).

Filkorn, ~~H. F.~~[H.F.](#), Scott, R., 2011. Microfossils, paleoenvironments and biostratigraphy of the Mal Paso Formation (Cretaceous, upper Albian), state of Guerrero, Mexico. Revista Mexicana de Ciencias Geológicas 28, 175–191.

Floquet, M., 1991. La plate-forme nord-castillane au Crétacé supérieur (Espagne): arrière-pays ibérique de la marge passive basco-cantabrique: sédimentation et vie. (Tesis Doctoral. Dijon). (in french, with english abstract).

Floquet, M., 1998. Outcrop cycle stratigraphy of shallow ramp deposits: the Late Cretaceous Series on the Castilian ramp (northern Spain). In: de Graciansky, P.C., Hardenbol, J., Jacquin, T., Vail, P.R. (Eds.), Mesozoic and Cenozoic Sequence Stratigraphy of European Basins. In: SEPM Spec. Publ, 60. pp. 343–361.

Floquet, M., 2004. El Cretácico Superior de la Cuenca Vasco-Cantábrica y áreas adyacentes. In: Vera, J.A. (Ed.), Geología de España. Sociedad Geológica de España and Instituto Geológico y Minero de España, Madrid, pp. 299–306.

Floquet, M., Alonso, A., Meléndez, A., 1982. Cameros-Castilla. El Cretácico superior. In: Universidad Complutense de Madrid and CSIC (Ed.), El Cretácico de España. Editorial Universidad Complutense de Madrid, Madrid, pp. 387–456 (in spanish).

Flügel, E., Munnecke, A., 2010. ~~Microfacies of carbonate rocks: analysis, interpretation and application~~[Microfacies of Carbonate Rocks: Analysis, Interpretation and Application](#). Springer, Berlin (976 pp.).

Frijia, G., Parente, M., Di Lucia, M., Mutti, M., 2015. Carbon and strontium isotope stratigraphy of the Upper Cretaceous (Cenomanian-Campanian) shallow-water carbonates of southern Italy: Chronostratigraphic calibration of larger foraminifera biostratigraphy. *Cretaceous Research* 53, 110–139. doi:10.1016/j.cretres.2014.11.002.

García, A., Mas, R., Segura, M., Carenas, B., García-Hidalgo, J.F., Gil, J., Alonso, A., Aurell, M., Bádenas, B., Benito, M.I., Meléndez, A., Salas, R., 2004. Segunda fase de post.rifting: Cretácico Superior. In: Vera, J.A. (Ed.), *Geología de España*. Sociedad Geológica de España and Instituto Geológico y Minero de España, Madrid, pp. 510–522 (in spanish).

Gil, J., Carenas, B., Segura, M., García-Hidalgo, J., García, A., 2004. Revisión y correlación de las unidades litoestratigráficas del Cretácico Superior en la región central y oriental de España. *Revista de la Sociedad Geológica de España* 17, 249–266 (in spanish, with english abstract).

Gil, J., García-Hidalgo, J., Segura, M., García, A., Carenas, B., 2006. Stratigraphic architecture, palaeogeography and sea-level changes of a third order depositional sequence: the late Turonian–early Coniacian in the northern Iberian Ranges and Central System (Spain). *Sedimentary Geology* 191, 191–225.

Gil, J., García-Hidalgo, J., Mateos, R., Segura, M., 2009. ~~orbital cycles in a Late Cretaceous shallow platform (Iberian Ranges, Spain)~~[Orbital cycles in a Late Cretaceous shallow platform \(Iberian Ranges, Spain\)](#). *Palaeogeography, Palaeoclimatology, Palaeoecology* 274, 40–53.

González, A., Guimerá, Y., 1993. Sedimentación sintectónica en una cuenca transportada sobre una lámina. *Revista de la Sociedad Geológica de España* 6, 1–2 (in spanish, with english abstract).

Gräfe, [K. U. K. U.](#), 1994. ~~Sequence stratigraphy in the Cretaceous and Paleogene (Aptian to Eocene) of the Basco-Cantabrian Basin (N. Spain)~~[Sequence Stratigraphy in the Cretaceous and Paleogene \(Aptian to Eocene\) of the Basco-Cantabrian Basin \(N. Spain\)](#). In: *Tübinger Geowissenschaftliche Arbeiten*, 18. Institut und Museum für Geologie und Paläontologie der Universität Tübingen Doctoral dissertation. (418 pp.).

Gräfe, K.U., 1999. ~~Sedimentary cycles, burial history and foraminiferal indicators for systems tracts and sequence boundaries in the Cretaceous of the Basco-Cantabrian Basin (northern Spain)~~[Sedimentary Cycles, Burial History and Foraminiferal Indicators for Systems Tracts and Sequence Boundaries in the Cretaceous of the Basco-Cantabrian Basin \(Northern Spain\)](#). In: *Neues Jahrbuch für Geologie und Paläontologie Abhandlungen*, 212. pp. 85–130.

Gräfe, K.U., 2005. Foraminíferos bentónicos del Cretácico Superior de la Cuenca Vasco-Cantábrica, Norte de España. *Journal of Iberian Geology* 277–299 (in spanish).

Haq, B.U., 2014. Cretaceous eustasy revisited. *Global and Planetary Change* 113, 44–58.

Hay, W.W., Floegel, S., 2012. New thoughts about the Cretaceous climate and oceans. *Earth-Science Reviews* 115, 262–272.

Heckel, [P. H. P. H.](#), 1974. Carbonate buildups in the geologic record: a review. In: Laporte, L.F. (Ed.), *Reefs in Time and Space*. In: *Soc. Econ. Paleontol. Mineral*, 18. pp. 90–154.

Hofmann, P., Wagner, T., Beckmann, B., 2003. Millennial-to centennial-scale record of African climate variability and organic carbon accumulation in the Coniacian–Santonian eastern tropical Atlantic (Ocean Drilling Program Site 959, off Ivory Coast and Ghana). *Geology* 31, 135–138.

Iannace, A., Frijia, G., Galluccio, L., Parente, M., 2014. Facies and early dolomitization in Upper Albian shallow-water carbonates of the southern Apennines (Italy): paleotectonic and paleoclimatic implications.

Joo, ~~Y.-J.Y.J.~~, Sageman, ~~B.-B.B.B.~~, 2014. Cenomanian to Campanian carbon isotope chemostratigraphy from the Western Interior Basin, USA. *Journal of Sedimentary Research* 84, 529–542.

Kauffman, ~~E.-G.E.G.~~, Johnson, ~~C.-C.C.C.~~, 1988. The morphological and ecological evolution of Middle and Upper Cretaceous reef-building rudistids. *Palaios* 194–216.

Knaust, D., Curran, ~~H.-A.H.A.~~, Dronov, ~~A.-V.A.V.~~, 2012. Shallow-marine carbonates. In: Knaust, ~~ÐÐ.~~, Bromley, R.G. (Eds.), ~~Trace fossils as indicators of sedimentary environments: developments in Sedimentology~~Trace Fossils as Indicators of Sedimentary Environments: Developments in Sedimentology. Elsevier, Amsterdam, pp. 705–750.

Kuhnt, W., Chellai, ~~E.-H.E.H.~~, Holbourn, A., Luderer, F., Thurow, J., Wagner, T., Kawamura, H., 2001. ~~Centennial records of Cretaceous paleoceanographic events and sea-level fluctuations in the Moroccan Tarfaya-Layoune basin~~Centennial Records of Cretaceous Paleoceanographic Events and Sea-level Fluctuations in the Moroccan Tarfaya-Layoune Basin. In: EOS Transactions, American Geophysical Union, 82, p. 32.

Lacovara, ~~K.-J.K.J.~~, Smith, ~~J.-R.J.R.~~, Smith, ~~J.-B.J.B.~~, Lamanna, ~~M.-C.M.C.~~, 2003. ~~The ten-thousand islands coast of Florida: A modern analog to low-energy mangrove coasts of cretaceous epeiric seas~~The Ten Thousand Islands Coast of Florida: A Modern Analog to Low-energy Mangrove Coasts of Cretaceous Epeiric Seas. In: ~~5th international conference on coastal sediments~~5th International Conference on Coastal Sediments. World Scientific Publishing Corporation and East Meets West Productions, Clearwater beach, Florida, pp. 1773–1784.

Laporte, ~~L.-F.L.F.~~, 1967. ~~Carbonate deposition near mean sea-level and resultant facies mosaie: Manlius Formation (Lower Devonian) of New York State~~Carbonate deposition near mean sea-level and resultant facies mosaie: Manlius Formation (lower Devonian) of New York State. *American Association of Petroleum Geologists Bulletin* 51, 73–101.

Le Goff, J., Cerepi, A., Ghysels, G., Swennen, R., Loisy, C., Heba, G., Muska, K., 2015. Meter-scale cycles as a proxy for the evolution of the Apulian Carbonate Platform during the late Cretaceous (Llogara Pass, Albania). *Facies* 61, 1–26.

Liu, K., 2007. Sequence stratigraphy and orbital cyclostratigraphy of the Mooreville Chalk (Santonian–Campanian), northeastern Gulf of Mexico area, USA. *Cretaceous Research* 28, 405–418.

Martín-Chivelet, J., 1995. Sequence stratigraphy of mixed carbonate-siliciclastic platforms developed in a tectonically active setting, Upper Cretaceous, Betic continental margin (Spain). *Journal of Sedimentary Research* 65, 235–254.

Martín-Chivelet, J., 2003. Quantitative analysis of accommodation patterns in carbonate platforms: an example from the mid-Cretaceous of SE Spain. *Palaeogeography, Palaeoclimatology, Palaeoecology* 200, 83–105.

Martín-Chivelet, J., Giménez, R., 1992. Palaeosols in microtidal carbonate sequences, Sierra de Utiel Formation, Upper Cretaceous, SE Spain. *Sedimentary Geology* 81, 125–145.

Martín-Chivelet, J., Berástegui, X., Rosales, I., Vilas, L., Vera, ~~J.-A.J.A.~~, Caus, E., Segura, M., 2002. Cretaceous. In: Gibbons, W., Moreno, T. (Eds.), *The Geology of Spain*. The Geological Society, London, pp. 255–292.

- Martín-Chivelet, J., Floquet, M., García-Senz, J., Callapez, [P.-M.P.M.](#), López-Mir, B., Muñoz, [J.-A.J.A.](#), Dinis, [P.-M.P.M.](#), 2019. Late Cretaceous post-rift to convergence in Iberia. In: [The geology of Iberia: a geodynamic approach](#)[The Geology of Iberia: A Geodynamic Approach](#). Springer, Cham, pp. 285–376.
- Masse, J., Fenerci, M., Pernarcic, E., 2003. Palaeobathymetric reconstruction of peritidal carbonates: Late Barremian, Urgonian, sequences of Provence (SE France). *Palaeogeography, Palaeoclimatology, Palaeoecology* 200, 65–81.
- McArthur, [J.-M.J.M.](#), Howarth, R., Shields, G., Zhou, Y., 2020. Strontium isotope stratigraphy. In: Gradstein, [F.-M.F.M.](#), Ogg, [J.-G.J.G.](#), Schmitz, [M.-D.M.D.](#), Ogg, [G.-M.G.M.](#) (Eds.), *Geologic Time Scale*. Elsevier, Amsterdam, pp. 211–238.
- Miller, [G.-H.G.H.](#), Wolfe, [A.-P.A.P.](#), Briner, [J.-P.J.P.](#), Sauer, [P.-E.P.E.](#), Nesje, A., 2005. Holocene glaciation and climate evolution of Baffin Island, Arctic Canada. *Quaternary Science Reviews* 24, 1703–1721.
- Miller, [C.-R.C.R.](#), James, [N.-P.N.P.](#), Kyser, [F.-K.T.K.](#), 2013. Genesis of blackened limestone clasts at late Cenozoic subaerial exposure surfaces, southern Australia. *Journal of Sedimentary Research* 83, 339–353.
- Moro, A., Skelton, [P.-W.P.W.](#), Čosović, V., 2002. Palaeoenvironmental setting of rudists in the Upper Cretaceous (Turonian–Maastrichtian) Adriatic Carbonate Platform (Croatia), based on sequence stratigraphy. *Cretaceous Research* 23, 489–508. doi:10.1006/cres.2002.1017.
- Nieto, L., Reolid, M., Rodríguez-Tovar, F., Castro, J., Molina, J., Ruiz-Ortiz, P., 2018. An integrated analysis (microfacies and ichnology) of a shallow carbonate-platform succession: upper Aptian, Lower Cretaceous, Betic Cordillera. *Facies* 64, 1–21.
- Pérez-Valera, F., Pérez-López, A., 2008. Stratigraphy and sedimentology of Muschelkalk carbonates of the Southern Iberian Continental Palaeomargin (Siles and Cehegín Formations, Southern Spain). *Facies* 54, 61–87.
- Pettijohn, [F.-J.F.J.](#), Potter, [P.-E.P.E.](#), Siever, R., 2012. [Sand and sandstone: Springer Science and Business Media](#)[Sand and Sandstone: Springer Science and Business Media](#). Springer-Verlag, New York (618 pp.).
- Pittet, B., Van Buchem, [F.-S.F.S.](#), Hillgärtner, H., Razin, P., Grötsch, J., Droste, H., 2002. Ecological succession, palaeoenvironmental change, and depositional sequences of Barremian–Aptian shallow-water carbonates in northern Oman. *Sedimentology* 49, 555–581.
- Pratt, B., 2010. Peritidal carbonates. In: James, P., Dalrymple, R.W. (Eds.), *Facies Models 4*. Geological Association of Canada, St. John's, pp. 401–420.
- Pratt, [B.-R.B.R.](#), Haidl, [F.-M.F.M.](#), Holmden, C., 2008. [Microbial patch reefs in Upper Ordovician Red River strata, Williston Basin, Saskatchewan: signal of heating in a deteriorating epeiric sea](#)[Microbial Patch Reefs in Upper Ordovician Red River Strata, Williston Basin, Saskatchewan: Signal of Heating in a Deteriorating Epeiric Sea](#). In: [Dynamics of epeiric seas](#)[Dynamics of Epeiric Seas](#), 48. pp. 303–340.
- Pucéat, E., Lécuyer, C., Sheppard, [S.-M.S.M.](#), Dromart, G., Reboulet, S., Grandjean, P., 2003. Thermal evolution of Cretaceous Tethyan marine waters inferred from oxygen isotope composition of fish tooth enamels. *Paleoceanography* 18.
- Reading, [B.-G.B.G.](#), 1978. [Sedimentary environments and facies](#)[Sedimentary Environments and Facies](#). Blackwell Scientific Publications, Oxford (615 pp.).
- Riding, R., 2002. Structure and composition of organic reefs and carbonate mud mounds: concepts and categories. *Earth-Science Reviews* 58, 163–231.

Rodríguez, L.R., López-Olmedo, F., Oliveira, J.T., Medialdea, T., Terrinha, P., Matas, J., Martín-Serrano, A., Martín-Parra, L.M., Rubio, F., Marín, C., Montes, Montes, M., Nozal, F., 2008. In: Rodríguez, L.R., Oliveira, J.T. (Eds.), Mapa Geológico de España y Portugal. In: Instituto geológico y minero de España and Laboratorio nacional de energía y geología de Portugal.

Salas, R., Guimerà, J., Mas, R., Martín-Closas, C., Meléndez, A., Alonso, A., 2001. Evolution of the Mesozoic central Iberian Rift System and its Cainozoic inversion (Iberian chain). *Mémoires du Museum national d'Histoire naturelle* 6, 145–185.

Sánchez-Moya, Y., Sopena, A., 2004. El Rift Mesozoico Ibérico. In: Vera, J.A. (Ed.), *Geología de España*. Sociedad Geológica de España and Instituto Geológico y Minero de España, Madrid, pp. 484–522 (in Spanish).

Scotese, ~~C. R.C.R.~~, Song, H., Mills, ~~B. J.B.J.~~, van der Meer, ~~D. G.D.G.~~, 2021. ~~Phanerozoic paleotemperatures: The earth's changing climate during the last 540 million years~~[Phanerozoic paleotemperatures: the earth's changing climate during the last 540 million years](#). *Earth-Science Reviews* 215, 103–503.

Segura, M., Carenas, B., Gil, J., García-Hidalgo, ~~J.F.J.F.~~, García, A., 2001. Anatomy of the carbonate bodies in relation to their position with respect to the maximum transgressive in the 2nd-order cycles of the Upper Cretaceous from the Iberian Range. *Géologie Méditerranéenne* 28, 163–168.

Segura, M., García Hidalgo, ~~J.F.J.F.~~, Carenas, B., Gil, J., García, A., 2004. Evolución paleogeográfica de la Cuenca Ibérica en el Cretácico Superior. *Geogaceta* 36, 103–116.

Segura, M., Barroso-Barcenilla, F., Callapez, P., García-Hidalgo, J., Gil-Gil, J., 2014. Depositional sequences and ammonoid assemblages in the upper Cenomanian-lower Santonian of the Iberian Peninsula (Spain and Portugal). *Geologica Acta* 12, 19–27.

Sevillano, A., Bádenas, B., Rosales, I., Barnolas, A., López-García, ~~J.M.J.M.~~, 2020. Orbital cycles, differential subsidence and internal factors controlling the high-frequency sequence architecture in a Sinemurian shallow carbonate platform (Mallorca island, Spain). *Sedimentary Geology* 407, 105–729. doi:10.1016/j.sedgeo.2020.105729.

Q12 Sevillano, A., Rosales, I., Barnolas, A., Bádenas, B., López-García, ~~J.M.J.M.~~, 2021. Revisión estratigráfica del Sinemuriense-Pliensbachiense inferior de Mallorca. *Estudios Geológicos* 77, 142 (in Spanish).

Shier, ~~D. E.D.E.~~, 1969. Vermetid reefs and coastal development in the Ten Thousand Islands, southwest Florida. *Geological Society of America Bulletin* 80, 485–508.

Shinn, E., 1983. Birdseyes, fenestrae, shrinkage pores, and loferites; a reevaluation. *Journal of Sedimentary Research* 53, 619–628.

Simone, L., Carannante, G., Ruberti, D., Sirna, M., Sirna, G., Laviano, A., Tropeano, M., 2003. Development of rudist lithosomes in the Coniacian–Lower Campanian carbonate shelves of central-southern Italy: high-energy vs low-energy settings. *Palaeogeography, Palaeoclimatology, Palaeoecology* 200, 5–29. doi:10.1016/s0031-0182(03)00442-5.

Skelton, ~~P.W.P.W.~~, 2003. Rudist evolution and extinction - a North African perspective. In: Gili, E., Negra, ~~M. E. H.M.E.H.~~, Skelton, ~~P.W.P.W.~~ (Eds.), ~~North African Cretaceous carbonate platform systems~~[North African Cretaceous Carbonate Platform Systems](#). Springer, Dordrecht, pp. 215–227.

Solak, C., Tash, K., Koç, H., 2017. ~~Biostratigraphy and facies analysis of the Upper Cretaceous–Danian? platform carbonate succession in the Kuyucak area, western Central Taurides, S Turkey~~Biostratigraphy and facies analysis of the Upper Cretaceous–Danian? Platform carbonate succession in the Kuyucak area, western Central Taurides, S Turkey. *Cretaceous Research* 79, 43–63. doi:10.1016/j.cretres.2017.06.019.

Stampfli, ~~G. M.G.M.~~, Kozur, ~~H. W.H.W.~~, 2006. Europe from the Variscan to the Alpine cycles. *Memoirs-Geological Society of London* 32, 57.

Steuber, T., Rauch, M., Masse, J.-P., Graaf, J., Malkoč, M., 2005. Low-latitude seasonality of Cretaceous temperatures in warm and cold episodes. *Nature* 437, 1341–1344.

Strasser, A., 1984. Black-pebble occurrence and genesis in Holocene carbonate sediments (Florida Keys, Bahamas, and Tunisia). *Journal of Sedimentary Research* 54, 1097–1109.

Sutherland, ~~P. K.P.K.~~, Henry, ~~T. W.T.W.~~, 1977. Carbonate platform facies and new stratigraphic nomenclature of the Morrowan Series (Lower and Middle Pennsylvanian), northeastern Oklahoma. *Geological Society of America Bulletin* 88, 425–440.

Taberner, M., Bosence, D., 1995. An Eocene Biodetrital Mud-Mound from the Southern Pyrenean Foreland Basin, Spain: An Ancient Analogue for Florida Bay Mounds? In: Monty, C.L.V., Bosence, D.W.J., Bridges, P.H., Pratt, B.R. (Eds.), *Carbonate Mud-Mounds, Their Origin and Evolution*, Spec. In: Publ. Int. Assoc. Sedimentol. Blackwell, Oxford, pp. 421–437.

Takashima, R., Nishi, H., Yamanaka, T., Hayashi, K., Waseda, A., Obuse, A., Letters, ~~P. S.P.S.~~, 2010. High-resolution terrestrial carbon isotope and planktic foraminiferal records of the Upper Cenomanian to the Lower Campanian in the Northwest Pacific. *Earth and Planetary Science Letters* 289, 570–582.

Tanner, ~~W. F.W.F.~~, 1960. Florida coastal classification. In: *Transactions - Gulf Coast Association of Geological Societies*, 10. pp. 259–266.

~~Tedesco, L., Wanless, H., 1990. Role of burrow excavation and infilling in creating the preserved depositional fabric of the core facies of modern and Paleozoic mud mounds. In: 13th International Association of Sedimentologists Annual Meeting, Nottingham, England. p. 214.~~

Thibault, N., Jarvis, I., Voigt, S., Gale, A., Attree, K., Jenkyns, H., 2016. Astronomical calibration and global correlation of the Santonian (Cretaceous) based on the marine carbon isotope record. *Paleoceanography* 31, 847–865.

Uličný, D., Jarvis, I., Gröcke, D., Čech, S., Laurin, J., Olde, K., Pedentchouk, N., 2014. A high-resolution carbon-isotope record of the Turonian stage correlated to a siliciclastic basin fill: Implications for mid-Cretaceous sea-level change. *Palaeogeography, Palaeoclimatology, Palaeoecology* 405, 42–58.

Val, J., Aurell, M., Badenas, B., Castanera, D., Subias, S., 2019. ~~Cyclic carbonate-siliciclastic sedimentation in a shallow marine to coastal environment (latest Kimmeridgian-early Tithonian, Galve sub-basin, Spain)~~Cyclic carbonate-siliciclastic sedimentation in a shallow marine to coastal environment (latest Kimmeridgian–Early Tithonian, Galve sub-basin, Spain). *Journal of Iberian Geology* 45, 195–222.

Van Wagoner, J., Posamentier, H., Mitchum, R., Vail, P., Sarg, J., Loutit, T., Hardenbol, J., 1988. An overview of the fundamentals of sequence stratigraphy and key definitions. An overview of sequence stratigraphy and key definitions. In: Wilgus, C.K., Hastings, ~~B. S.B.S.~~, Kendall, C.G.St.C., Posamentier, H.W., Ross, C.A., Van Wagoner, ~~J. C.J.C.~~ (Eds.), *Sea Level Changes—An Integrated Approach*. In: SEPM Special Publication, 42. pp. 39–45 Oklahoma.

Velić, I., 2007. Stratigraphy and Palaeobiogeography of Mesozoic Benthic Foraminifera of the Karst Dinarides (SE Europe)-PART 1. *Geologia Croatica* 60, 1–60.

Vicens, E., López, G., Obrador, A., 1998. Facies succession, biostratigraphy and rudist faunas of Coniacian to Santonian platform deposits in the Sant Corneli anticline (Southern Central Pyrenees). *Geobios* 31, 403–427.

Villalba-Breva, S., Martín-Closas, C., 2013. Upper Cretaceous paleogeography of the Central Southern Pyrenean Basins (Catalonia, Spain) from microfacies analysis and charophyte biostratigraphy. *Facies* 59, 319–345.

Wang, J.D., van de Kreeke, J., Krishnan, N., Smith, D., 1994. Wind and tide response in Florida Bay. *Bulletin of Marine Science* 54, 579–601.

Wanless, H., Cottrell, D., Tagett, M., Tedesco, L., Warzeski, E., 1995. Origin and growth of carbonate banks in south Florida C.L.V. In: Monty, Bosence, D.W.J., Bridges, P.H., Pratt, B.R. (Eds.), *Carbonate Mud-Mounds, Their Origin and Evolution*. In: ~~Spec. Publ. Int. Assoc. Sedimentol.~~ Special Publication of the International Association Sedimentology. Blackwell, Oxford, pp. 439–473.

Wendler, ~~J.-E.~~ J.E., Wendler, I., 2016. What drove sea-level fluctuations during the mid-Cretaceous greenhouse climate? *Palaeogeography, Palaeoclimatology, Palaeoecology* 441, 412–419.

Wingard, ~~G.-L.~~ G.L., Bergstresser, ~~S.-E.~~ S.E., Stackhouse, B., Jones, M., Marot, ~~M.-E.~~ M.E., Hoefke, K., 2020. Impacts of Hurricane Irma on Florida Bay Islands, Everglades National Park, USA. *Estuaries and Coasts* 43, 1070–1089.

Wu, H., Zhang, S., Hinnov, ~~L.-A.~~ L.A., Jiang, G., Yang, T., Li, H., Wang, C., 2014. ~~Cyclostratigraphy and orbital tuning of the terrestrial upper Santonian–Lower Danian in Songliao Basin, northeastern China~~ Cyclostratigraphy and orbital tuning of the terrestrial Upper Santonian–Lower Danian in Songliao Basin, northeastern China. *Journal of Earth Planetary Science Letters* 407, 82–95.

Highlights

- La Cañadilla Fm deposited in a carbonate mud-dominated coastal plain to lagoon
- A transitional facies belt with mudbanks and ponds is compared to Florida analogues.
- A mid Santonian-early Campanian age is precised by strontium data.
- Sea-level changes driven by eccentricity cycles had major control in sedimentation.

Queries and Answers

Q1

Query: Your article is registered as a regular item and is being processed for inclusion in a regular issue of the journal. If this is NOT correct and your article belongs to a Special Issue/Collection please contact p.rajendran.1@elsevier.com immediately prior to returning your corrections.

Answer: Yes

Q2

Query: Please confirm that given names and surnames have been identified correctly and are presented in the desired order, and please carefully verify the spelling of all authors' names.

Answer: Yes

Q3

Query: The author names have been tagged as given names and surnames (surnames are highlighted in teal color). Please confirm if they have been identified correctly.

Answer: Yes

Q4

Query: Citation "Aurell et al., 2021" has not been found in the reference list. Please supply full details for this reference.

Answer: It was a mistake, we have deleted the Aurell et al., 2021 reference.

Q5

Query: The citation "Skelton et al. 2003" has been changed to "Skelton, 2003" to match the author name/date in the reference list. Please check if the change is fine in this occurrence and modify the subsequent occurrences, if necessary.

Answer: it is fine

Q6

Query: The citation "Flügel (2010)" has been changed to "Flügel and Munnecke (2010)" to match the author name/date in the reference list. Please check if the change is fine in this occurrence and modify the subsequent occurrences, if necessary.

Answer: it is fine

Q7

Query: Please note that Fig. 12 was not cited in the text. Please check if the suggested citation is appropriate, and correct if necessary.

Answer: Fig.12 was in fact originally cited in 5.1 section, after some changes we accidentally deleted it. I moved your proposed cite to its original position.

Q8

Query: The citation "Bosence 1990" has been changed to "Bosence and Waltham, 1990" to match the author name/date in the reference list. Please check if the change is fine in this occurrence and modify the subsequent occurrences, if necessary.

Answer: it is fine

Q9

Query: The citation "Val et al., 2018" has been changed to "Val et al., 2019" to match the author name/date in the reference list. Please check if the change is fine in this occurrence and modify the subsequent occurrences, if necessary.

Answer: it is fine

Q10

Query: Uncited reference: This section comprises references that occur in the reference list but not in the body of the text. Please position each reference in the text or, alternatively, delete it. Thank you.

Answer: We decided to delete this reference during reviews, but forget to delete it from the reference list. It has been done now.

Q11

Query: Have we correctly interpreted the following funding source(s) and country names you cited in your article: "Spanish Ministry of Science and Innovation; European Regional Development Fund; Government of Aragón; DGA Grant".

Answer: Yes

Q12

Query: Last page number has been deleted in reference "Sevillano et al., 2021" as it's identical with the first page number. Please check if it is appropriate.

Answer: it is appropriate